iScience

CellPress

Article

Roughness of Transmembrane Helices Reduces Lipid Membrane Dynamics

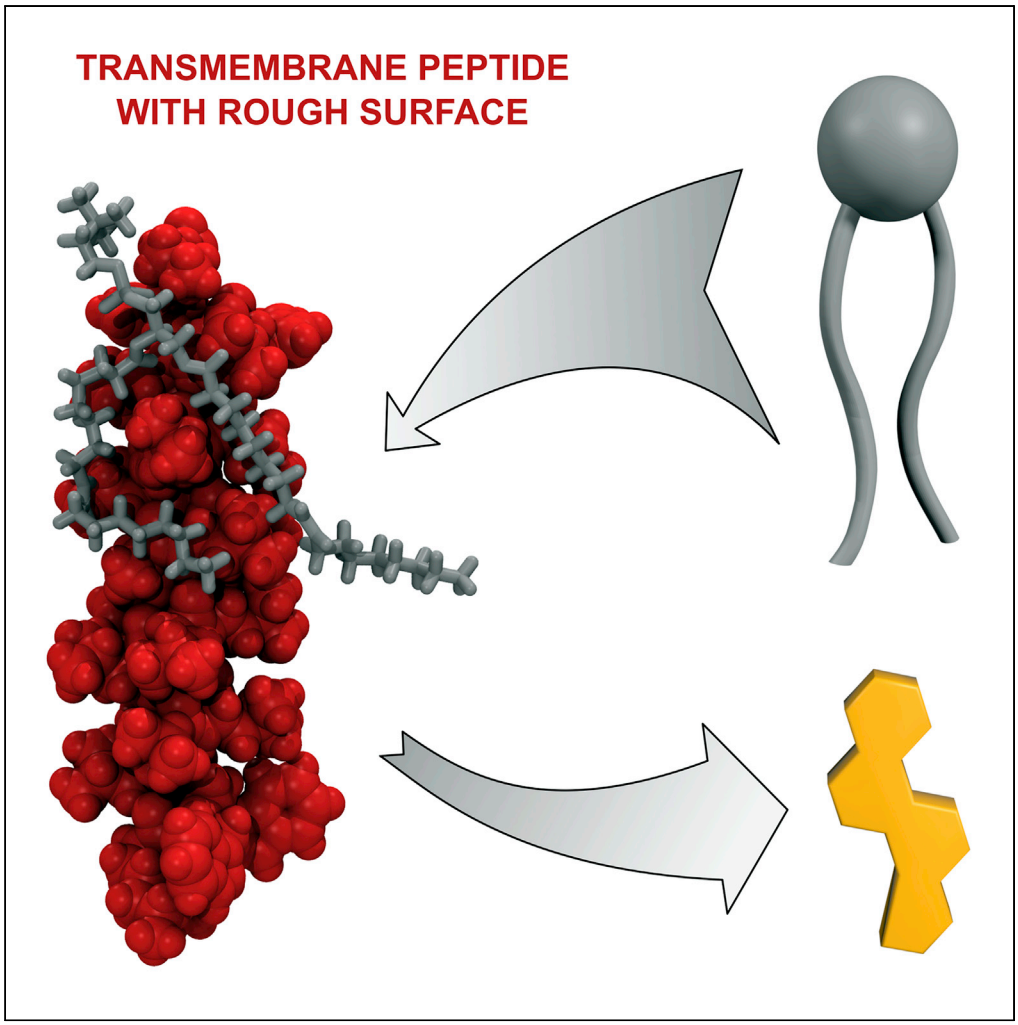

Marie Olšinová, Piotr Jurkiewicz, Iryna Kishko, ..., Martin Hof, Lukasz Cwiklik, Marek Cebecauer

marek.cebecauer@jh-inst.cas.cz

HIGHLIGHTS

Integral proteins densely populate cellular membranes

The rough surface of their transmembrane segment traps lipid acyl chains in membranes

Cholesterol segregates from transmembrane segments of proteins

Lateral mobility is reduced in protein-rich membranes

Olšinová et al., iScience *10*, 87–97
December 21, 2018
https://doi.org/10.1016/j.isci.2018.11.026

iScience

CellPress

Article

Roughness of Transmembrane Helices Reduces Lipid Membrane Dynamics

Marie Olšinová,[1,3] Piotr Jurkiewicz,[1] Iryna Kishko,[1] Jan Sýkora,[1] Ján Sabó,[1] Martin Hof,[1] Lukasz Cwiklik,[2] and Marek Cebecauer[1,4,*]

SUMMARY

The dynamics of cellular membranes is primarily determined by lipid species forming a bilayer. Proteins are considered mainly as effector molecules of diverse cellular processes. In addition to large assemblies of proteins, which were found to influence properties of fluid membranes, biological membranes are densely populated by small, highly mobile proteins. However, little is known about the effect of such proteins on the dynamics of membranes. Using synthetic peptides, we demonstrate that transmembrane helices interfere with the mobility of membrane components by trapping lipid acyl chains on their rough surfaces. The effect is more pronounced in the presence of cholesterol, which segregates from the rough surface of helical peptides. This may contribute to the formation or stabilization of membrane heterogeneities. Since roughness is a general property of helical transmembrane segments, our results suggest that, independent of their size or cytoskeleton linkage, integral membrane proteins affect local membrane dynamics and organization.

INTRODUCTION

Membranes support many vital functions of living cells. Diverse lipid species form the structural basis of cellular membranes. Lipids are also the main determinants of a membrane's physical properties (e.g., fluidity and continuity), which, in turn, influence the probability of the intermolecular interactions of its constituents (Bernardino de la Serna et al., 2016). On the other hand, proteins are key effectors involved in membrane-associated processes such as cell adhesion, signaling, and metabolism. Proteins constitute up to 50% of the total membrane mass (Dupuy and Engelman, 2008). A large part of these proteins is fully integrated into the hydrophobic core of membranes via one or more transmembrane domains (TMDs), which are in direct contact with lipids. This presents an important question: "How do integral proteins influence membrane properties"?

Detailed data are available on how the lipid composition, temperature, and surrounding environment (e.g., ions) influence membrane properties and organization in the absence of proteins (for review, see Heberle and Feigenson, 2011). However, little is known about these parameters when integrated peptides or proteins are present in lipid membranes. Structural studies of membrane proteins have suggested extensive trapping of lipid acyl chains at the surface of the transmembrane (TM) segments (Hite et al., 2010), but do not provide any insight into the more general consequences of this phenomenon. Early spectroscopy measurements (electron paramagnetic resonance or electron spin resonance spectroscopy [EPR/ESR] and nuclear magnetic resonance [NMR]) uncovered the existence of annular (or boundary) lipids forming the first shell surrounding the TM segments of membrane proteins (Brotherus et al., 1981; Jost et al., 1973, 1977; Bienvenue et al., 1982). Annular lipids exhibit restricted rotational mobility, slower exchange rates, and altered conformational order of acyl chains compared with the lipids in protein-free membranes (Marsh, 2008). Such altered lipid properties were observed for the first shell, but did not extend to the lipids of the bulk membrane (for the review, see Marsh, 2008). Moreover, in these experiments, the lipid annulus was easily detected when large, multispanning proteins (e.g., rhodopsin or cytochrome *c* oxidase) were tested. On the contrary, only small changes in the physical properties of annular lipids were detected in membranes containing simple TM peptides, and these were largely attributed to hydrophobic mismatch (Marsh, 2008; de Planque et al., 1998, 1999). This phenomenon is caused by the mismatch between the length of a hydrophobic peptide and the thickness of the membrane's hydrophobic core. The mismatch leads to the deformation of lipid acyl chains and, possibly, the formation of lipid domains (de Planque and Killian, 2003; Anderson and Jacobson, 2002; Mouritsen and Bloom, 1984). These spectroscopic data, supported by fluorescence quenching experiments (London and Feigenson, 1981), led to the conclusion that large integral proteins, with their hard surface and low mobility, affect lipid dynamics in membranes, including those in cells (Marsh, 2008; Nyholm, 2015). It is important to note that

[1]Department of Biophysical Chemistry, J. Heyrovsky Institute of Physical Chemistry of the Czech Academy of Sciences, Dolejškova 3, 182 23 Prague, Czech Republic

[2]Department of Theoretical Chemistry, J. Heyrovsky Institute of Physical Chemistry of the Czech Academy of Sciences, Dolejškova 3, 182 23 Prague, Czech Republic

[3]Present Address: Imaging Methods Core Facility at BIOCEV, Biology Section, Faculty of Science, Charles University, Průmyslová 595, 252 50 Vestec, Czech Republic

[4]Lead Contact

*Correspondence: marek.cebecauer@jh-inst.cas.cz

https://doi.org/10.1016/j.isci.2018.11.026

protein aggregation, formation of domains, and membrane multilamellarity, which may contribute to the measured changes in spectra, could not be controlled in these pilot works on proteo-membranes. The abovementioned spectroscopic techniques are also limited by narrow observation space and low hydration of tested samples.

Recent developments in fluorescence microscopic and spectroscopic techniques enabled more detailed physical characterization of fully hydrated, free-standing, and unilamellar membranes. Using fluorescence correlation spectroscopy (FCS), Ramadurai et al. measured the lateral diffusion of a set of purified proteins reconstituted in free-standing giant unilamellar vesicles (GUVs) and found that protein and lipid diffusion decreased linearly with increasing content of large, multispanning membrane proteins (Ramadurai et al., 2009). The results were interpreted as an impact of protein crowding, in agreement with existing theoretical predictions (Saxton, 1987). These conclusions were supported by calculated anomality parameters (α), but remain controversial owing to the low protein surface density of tested samples (<3,000 proteins/μm^2). The effect of obstacles is limited to large or immobile objects at high concentrations (Oppenheimer and Diamant, 2011). Low concentrations of proteins were used probably due to inefficient reconstitution of such large purified proteins in tested membranes. In addition, the proteins were mobile (Ramadurai et al., 2009). Furthermore, most proteins in cellular membranes are rather small (single spanners; Pieper et al., 2013). In their other two works, Ramadurai et al. again used FCS and well-defined membranes to demonstrate the altered diffusion of proteins in membranes with extensive hydrophobic mismatch (Ramadurai et al., 2010a, 2010b). The lateral mobility of both large membrane proteins and TM peptides of varying length was measured in membranes of different thickness. However, the effect of increased protein or peptide content in membranes was not tested in these studies. It is most likely that, in cellular membranes composed of a broad spectrum of lipid species, any temporary hydrophobic mismatch will be rapidly compensated by the lipids that match the TM segment of a protein. We were therefore interested in whether small, highly mobile proteins at near-physiological concentrations can influence membrane dynamics in the absence of previously described mechanisms such as protein crowding and aggregation or hydrophobic mismatch.

Cholesterol is an essential component of selected cellular membranes (van Meer et al., 2008). Its impact on protein-free membranes is well described (Mouritsen and Zuckermann, 2004). Cholesterol increases the rigidity of highly fluid, disordered membranes but has a disordering (fluidifying) effect on membranes composed of highly rigid lipids with low melting temperatures (T_m). The presence of cholesterol increases the membrane thickness (Gallova et al., 2004) and reduces the probability of membrane penetration by hydrophilic molecules (Raffy and Teissie, 1999). Very few studies have investigated protein- or peptide-containing membranes in the presence of cholesterol (Nystrom et al., 2010; Kaiser et al., 2011). It was shown there that increasing presence of TM peptides affects cholesterol partitioning into membranes (Nystrom et al., 2010) and, in a reverse setup, that increasing the concentration of cholesterol leads to the aggregation of TM peptides (Kaiser et al., 2011). These data indicate that TMDs of proteins can influence the properties of cholesterol-containing membranes, but they do not provide more detailed insight into the interrelation between TM segments of proteins and cholesterol. In this work, we tested the impact of a simple TM peptide on membrane dynamics in the absence and presence of physiological levels of cholesterol (25 mol %).

RESULTS

Reduced Lateral Diffusion and Increased Local Viscosity in Membranes with Helical Transmembrane Peptides

To investigate the direct impact of small and mobile TM proteins on membrane dynamics, we first adjusted our experimental model to minimize the impact of hydrophobic mismatch, molecular clusters, and crowding or membrane lipid domains on measured parameters. To comply with all these conditions, we focused on model membranes with only two components: α-helical TM peptides and phospholipids (Figure S1). The synthetic, highly purified TM peptide (LW21: GLLDSKKWWLLLLLLLALLLLLLLWWKKFSRS) and DOPC (dioleoyl phosphatidylcholine) were selected based on a number of prerequisites: (1) the peptide is monomeric and does not aggregate in DOPC membranes (Figure S2, Sparr et al., 2005), (2) there is no hydrophobic mismatch between the TM segment of the LW21 peptide and the thickness of DOPC membranes (Kaiser et al., 2011), (3) the LW21 peptide adopts a transbilayer orientation and α-helical structure in DOPC membranes (Kaiser et al., 2011; Machan et al., 2014), and (4) DOPC, with its low melting point of $-18.3^{\circ}C$, provides a highly fluid lipid environment with no detectable nanodomains in all tested vesicles

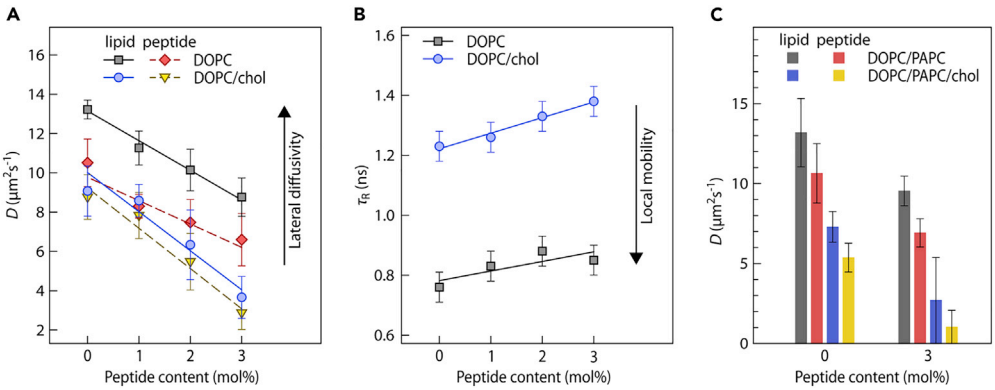

Figure 1. Impeded Local Viscosity and Lateral Diffusion in Membranes with Peptides

(A) Lateral diffusion coefficients of the lipid tracer (DiD; full lines) and fluorescently labeled LW21 peptide (dashed lines) were measured in GUVs composed of DOPC (black and red lines) and DOPC:cholesterol (75:25; blue and yellow lines) in the presence of increasing concentrations of unlabeled peptides. Each presented diffusion coefficient (*D*) was measured for at least 10 vesicles in three independent experiments using the calibration-free z-scan FCS technique. Error bars indicate standard deviations (SD).

(B) Local lipid mobility (viscosity) as a function of increasing peptide concentration was determined in the absence (black squares) or presence (blue circles) of 25 mol % cholesterol using a Laurdan fluorescent probe by TRES. The relaxation time τ_R reports on the local lipid mobility. Error bars represent intrinsic uncertainty of the method.

(C) Lateral diffusion coefficients of the lipid tracer (DiD; gray and blue bars) and fluorescently labeled LW21 peptide (red and yellow bars) were measured in GUVs composed of DOPC:PAPC (90:10; black and red bars) and DOPC:PAPC:cholesterol (65:10:25; blue and yellow bars), in the absence and presence (3 mol %) of the unlabeled peptide. Each presented diffusion coefficient (*D*) was measured for at least 8 vesicles in two independent experiments using calibration-free z-scan FCS technique. Error bars indicate SD.

in the absence and presence of 25 mol % cholesterol (Stefl et al., 2012). Importantly, LW21 and similar TM peptides have comparable size with lipids and are highly mobile in DOPC vesicles (Figure 1A; Ramadurai et al., 2009). Therefore, no crowding is expected in membranes composed of LW21 peptides and DOPC. Finally, we have selected these components to comply with the prevalent α-helical structure of TMDs and dominance of glycerophospholipids in mammalian cell membranes.

To our knowledge, no molar concentrations were experimentally determined for lipids and proteins in cell membranes to date. However, proteins were found to form around one-half of total mass in cellular membranes (Dupuy and Engelman, 2008). By considering a small size of lipids (~1 kDa) and an average size of proteins (~40 kDa; Brocchieri and Karlin, 2005), we estimate the molar concentration of proteins in cell membranes to be approximately 2.5 mol %. Therefore, we have examined free-standing model membranes (GUVs) containing 0–3 mol % of the LW21 peptide. The calibration-free *z*-scan FCS technique (Benda et al., 2003) was used to measure lateral diffusion of the fluorescent lipid tracer, DiD, and fluorescently labeled LW21 embedded in membranes. In Figure 1A, we demonstrate that increasing the concentration of the monomeric α-helical peptide reduced lateral diffusion of both the lipid tracer and labeled peptide (gray and red lines, respectively). At the highest tested peptide concentration, 3 mol %, the diffusivity of both molecules was reduced by approximately 35% in DOPC membranes. In agreement with the literature (Weiss et al., 2013), lipid molecules diffused somewhat faster than peptides at all tested peptide concentrations. The observed effect was comparable to the reduction of lateral mobility in membranes with the highest tested concentration of large, multispanning proteins (0.02–0.2 mol %; Ramadurai et al., 2009). However, no anomalous diffusion was observed for all tested compositions (Table S1). Next, the experiments were performed in the presence of 25 mol % cholesterol to better mimic cell membranes (van Meer et al., 2008). The peptide incorporates into membranes with and without cholesterol with comparable efficiency (Figures S3 and S4). The impact of the peptide on the lateral diffusion of membrane components was more pronounced in the presence of cholesterol than in its absence. At the highest peptide concentration, 3 mol %, we observed a 2- to 3-fold decrease in the diffusion coefficients for both tested molecules (Figure 1A). Quantitative analysis supports the enhanced effect of the peptide on the mobility of membrane components in the presence of cholesterol compared with its absence (D_{25}/D_0 values; Table S2). Importantly, lateral diffusion of lipids and peptides was indistinguishable in membranes with cholesterol

Membrane (Large Unilamellar Vesicles)	*S* (DOPC)	*S* (DOPC/Cholesterol)
DOPC	0.19 ± 0.06	0.43 ± 0.01
DOPC +3% LW21	0.28 ± 0.04	0.51 ± 0.05
DOPC +10% LW21	0.39 ± 0.02	0.55 ± 0.08

Table 1. Order Parameter *S* of DPH in Membranes with the LW21 Peptide and the Standard Deviation

(Figure 1A; blue and yellow lines). Again, no anomalous diffusion was observed in the presence of cholesterol (Table S1).

To characterize the physical properties of membranes containing peptides, we evaluated the dynamics of the peptide-containing membranes at the nanoscale using environment-sensitive fluorescent probes. First, the time-resolved emission spectra (TRES) of a Laurdan probe located at the interface of the hydrophobic and hydrophilic parts of the lipid bilayer at the level of lipid carbonyls were measured (Figure S5). The speed of Laurdan TRES red shift, represented by the relaxation time τ_R, reports on the local mobility of lipids. The total emission shift $\Delta\nu$ reflects hydration of tested membranes. Significant increase of τ_R as a function of the peptide content in DOPC membranes demonstrates that LW21 hinders lipid mobility (Figure 1B). The hindrance was slightly stronger in the presence of cholesterol compared with its absence (Figure 1B; linear regression slope of 0.05 versus 0.03, respectively), supporting a stronger effect of peptides on lateral diffusion in membranes with the sterol. Interestingly, $\Delta\nu$ values remained unchanged under all tested conditions (Table S3), indicating that the presence of the LW21 peptide does not disturb the structural integrity of lipid bilayer. Second, the time-resolved anisotropy of a diphenylhexatriene (DPH) probe was measured to characterize the order and mobility of lipid tails forming the hydrophobic interior of the membrane. The results show the restriction in DPH rotation manifested in the elevated DPH order parameter *S* in the presence of peptide (Table 1). This effect was preserved in cholesterol-containing membranes, which agrees with the previously published data (Nystrom et al., 2010).

Phospholipids in cellular membranes commonly contain two different fatty acids attached to their head groups, one of which is often polyunsaturated (Harayama and Riezman, 2018). Moreover, polyunsaturated acyl chains tend to preferentially associate with membrane proteins, especially in the presence of cholesterol (Polozova and Litman, 2000; Pitman et al., 2005). To evaluate whether TM peptides modulate the dynamics of membranes with polyunsaturated acyl chains, we measured the mobility of DiD and labeled the LW21 peptide in DOPC membranes containing 10 mol % of palmitoyl-arachidonoylphosphatidylcholine (PAPC). The results shown in Figure 1C demonstrate that the presence of the peptide (3 mol %) reduces the mobility of membrane components by approximately 35%, which is the level comparable to the membranes composed of only DOPC. Again, a greater effect was observed in the presence of 25 mol % cholesterol. The addition of 3 mol % of the LW21 peptide to the cholesterol- and PAPC-containing membranes caused a 2- to 4-fold reduction in the lateral mobility of lipid and peptide probes (Figure 1C). These data demonstrate that small, highly mobile proteins affect the dynamics of membranes containing hybrid lipids with one polyunsaturated acyl chain.

Trapping of Acyl Chains on the Rough Surfaces of Helical Transmembrane Peptides

To better understand the mechanism responsible for the reduced membrane dynamics observed in our experiments, we performed fully atomistic molecular dynamics (MD) simulations of the LW21 peptide in the lipid bilayers composed of DOPC (Video S1). The simulations were performed over 500 ns, including the first 200 ns used for the equilibration of the system. The data confirmed that the mobility of the lipids close to the peptide is severely impeded (Figure S6). Interestingly, we observed that this is caused by the rough surface of the peptide and the trapping of acyl chains of annular lipids in the grooves therein (Figures 2A and 2B). Such lipid-peptide contacts are nonspecific (Figure S7) and exhibit substantial stability (Figure 2C). Combined with our experimental data, these findings demonstrate that the mobility of lipids is affected not only by large, multispanning proteins, as reported in recent computational studies (Camley et al., 2010; Niemela et al., 2010), but also by much smaller objects such as a single TMD, owing to its rough surface. In the literature, TMDs are often represented by smooth cylinders (Figure 3A). However, stable helical peptides formed by native amino acids are intrinsically rough (Figure 3B). The rough surface is formed by amino acid side chains of helical peptides and is not limited to poly-leucine segments. Indeed,

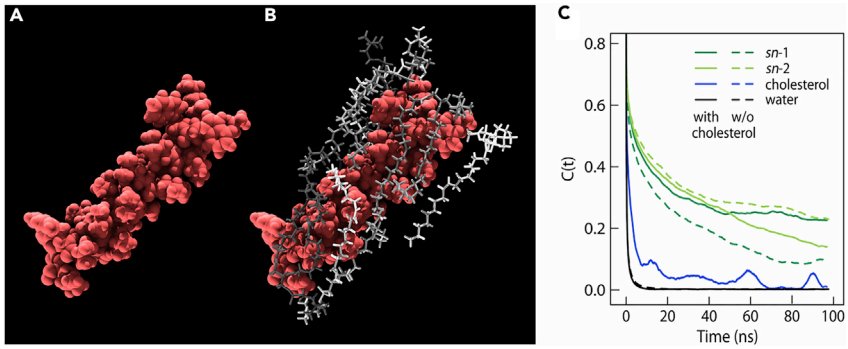

Figure 2. Lipid Acyl Chain Trapping on the Rough Surface of the LW21 Peptide

(A and B) A typical snapshot from MD simulation of the peptide in the DOPC bilayer, indicating trapping of lipid acyl chains in the grooves formed by peptide side chains. Peptide surface (A) is shown in red. Interacting lipids are shown in different shades of gray using licorice representation (B). Non-interacting lipids and water were removed for clarity. The molecular composition of the system characterized by the MD simulation is in Table S5.

(C) Autocorrelation functions of peptide backbone contact with individual acyl chains, cholesterol, and water in the membranes without and with 25 mol % of cholesterol. A cutoff of 0.75 nm was employed for the definition of contacts.

a rough surface has been observed in all TMDs of proteins characterized so far by X-ray crystallography or NMR at sufficient resolution (<4.5 Å; PDBTM database, http://pdbtm.enzim.hu/; Kozma et al., 2013).

The data acquired using the LW21 peptide could not be compared with a smooth variant because all α-helix-forming amino acids intrinsically form structures with a rough surface (Figure 3B). Therefore, we have generated coarse-grain toy models of cylinder-like objects with varying surface roughness (M1-M3; Figure 4A) that were embedded in DOPC membranes. The autocorrelation data acquired from MD simulations indicate longer lipid contacts with the rougher models (M3 > M2 > M1; Figure 4B). The acyl chains are entrapped in the grooves of rougher models (M2 and M3), which hinders their mobility (Figure S8). Virtually no trapping was observed on the smooth surface of model M1 (Figure 4B). These results are in agreement with previously published findings regarding the interference of nanoscopically rough surfaces composed of diverse synthetic materials on the mobility of polymers (Wang et al., 2015) and peptides (Shezad et al., 2016). This suggests that cylinder-like objects with rough surfaces embedded in membranes impede lipids similarly to the LW21 peptide.

Segregation of Cholesterol from the Rough Surface of Helical Transmembrane Peptides

We also performed MD simulations of the LW21 peptide in lipid bilayers composed of DOPC and 25 mol % cholesterol (Videos S2 and S3). We found cholesterol to be excluded from the peptide annulus for the full period of the simulations (500 ns), enabling phospholipid acyl chains to interact preferentially with the rough surface of the peptide (Figure 5). Only very rare and highly transient contacts of cholesterol with the peptide were detected (Figures 2C and 5B). This is probably caused by the incompatibility between the planar shape of cholesterol molecule and the roughness of helical TM peptides, which prefer the flexibility of phospholipid acyl chains (Figure 5F, compare to Figure 2B; Rog et al., 2007).

Interestingly, organization of phospholipids in the vicinity of the peptide and the trapping of their acyl chains on its rough surface remain unaffected in the absence and presence of cholesterol. This observation is supported by the detailed analysis of acyl chain order calculated from MD simulations wherein the lipids from the peptide annulus and those in the bulk (non-annular) can be analyzed separately (Figure 6 and Table S4). These data suggest that the overall mobility-reducing effect of peptides in the presence of cholesterol is probably caused by complex events: (1) the rough surface of the peptide causes lipid acyl chain trapping and the locally reduced lateral mobility of phospholipids (Figures 1A, 2B, and S6) and (2) cholesterol presence is strongly reduced in the peptide annulus (Figure 5; see also Rog et al., 2008; Pitman et al., 2005), which leads to (3) the increased concentration of cholesterol in the bulk of the lipid membrane and reduced lateral mobility (increased acyl chain order) therein (Figure 6). The last of these three is probably caused by the rigidifying effect of cholesterol itself as observed in peptide-free membranes (Mouritsen and Zuckermann, 2004). Therefore, the lipid acyl chain trapping at the rough surface of the peptide applies

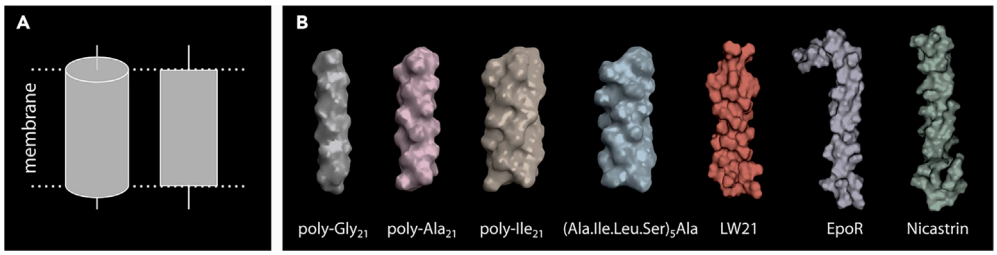

Figure 3. Rough Surface of Transmembrane Helices

(A) Common illustration styles representing TMDs as smooth cylinders.

(B) On the contrary, helical peptides have inherently rough surfaces formed by amino acid side chains. Poly-glycine, poly-alanine, and poly-isoleucine artificial helical peptides represent diverse sequences composed of single amino acid species. Excepting poly-glycine, all helices exhibit rough surfaces. Oligo-glycine alone does not support helical structure. The combination of amino acids AILS (blue-gray) indicates that the non-homogenous amino acid sequence forms even more extensive roughness. Surface representations for LW21 peptide and 2 TM domains (EpoR— PDB: 2MV6; and nicastrin— PDB: 2N7R) are shown for comparison. The structure of helical peptides (monogenic, AILS, and LW21) was modeled using surface visualization in PyMOL software. These structures do not represent calculated surfaces and are shown solely to indicate roughness of the surface for any combination of amino acids.

for both membranes with and without cholesterol. However, owing to the segregation of cholesterol, MD simulations indicate a different impact of the peptide on membranes with and without cholesterol. The peptide decelerates the dynamics of cholesterol-containing membranes due to a combined effect of its rough surface on phospholipids and cholesterol.

DISCUSSION

In this study, we have investigated how small, highly mobile TM proteins can influence membrane dynamics and organization under well-controlled conditions in synthetic model membranes. Our model system was selected to avoid the impact of factors that were previously shown to influence membrane properties, e.g., hydrophobic mismatch, protein crowding and clustering (aggregation), or formation of domains. This could not be achieved in cells or other complex model systems (e.g., cell-derived vesicles). The presence of a variety of chemical species together with active membrane processes provides cells with enormous adaptability, and the experimental conditions cannot be properly controlled externally. In addition to these previously described phenomena, which depend on specific membrane environment, we were interested in whether integral proteins, independent of their size and higher organization, possess some universal property that can directly modulate membrane dynamics. Our results demonstrate that the rough surface of TM protein segments decelerates membrane dynamics, especially in the presence of cholesterol. This effect has not been previously shown experimentally in a well-controlled, fully hydrated system, and the available fragmented data did not provide good basis for a universal model explaining how proteins can affect membranes.

The mobility of membrane molecules is described in the Saffman-Delbrück (S-D) hydrodynamic model (Saffman and Delbruck, 1975), which highlights the impact of viscosity and, partially, the size of molecules. The variants of the S-D model for large immobile objects (Oppenheimer and Diamant, 2011) or multispanners in heterogeneous lipid membranes (Camley et al., 2010) considered proteins (or their TMDs) to be smooth cylinders with an effective radius of >4 nm. The calculated effect of such objects on lateral diffusion was negligible at low concentrations (<5 mol %). In nature, a majority of proteins possess a single or very few TMDs (Pieper et al., 2013). Their effective intramembranous radius is thus more comparable to the size of lipids (~1 nm) than to large, multispanning proteins. Moreover, most of the tested proteins were highly mobile in cellular membranes with diffusivities of 0.001–0.1 $\mu m^2/s$ (Bernardino de la Serna et al., 2016; Jacobson et al., 1987). It is therefore important to verify whether small, highly mobile TM peptides (a model of a single TMD) at low, physiologically relevant concentrations (<5 mol %) modulate membrane dynamics. We demonstrate that such peptides reduce the diffusivity of membrane components by exposing their rough surface to the surrounding phospholipids. The effect is more pronounced in membranes containing physiological levels of cholesterol (25 mol %), which better mimic properties of the selected membranes of eukaryotic cells (e.g., plasma membrane, Golgi apparatus, and endosomes). This observation agrees with our toy model (Figure 4), showing that objects with rough surfaces have a stronger effect on membranes

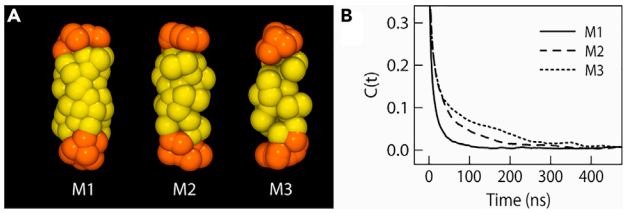

Figure 4. Rough Surface Interferes with Membrane Dynamics

(A) Toy models (M1–M3) of cylinder-like structures generated using a coarse-grain force field.

(B) The autocorrelation curves for contacts between lipid tails and the surface of model structures M1–M3 with increasing roughness embedded in DOPC membrane, indicating the trapping of acyl chains at the rough surface of M2 and M3. Similar effect was observed in the presence of 25 mol % cholesterol (Figure S9).

compared with smooth ones. The rough surface causes lipid acyl chain trapping, increased local viscosity, and, consequently, a reduction in lateral diffusion of membrane molecules.

We argue that this effect is not restricted to the peptide tested in this work because all amino acids, apart from glycine, form a rough surface when assembled in a helix (Figure 3B). Non-specific trapping of lipid acyl chains in the grooves on the surface of membrane proteins is a common finding in those crystallized in lipid membranes, for example, aquaporin-0 (Hite et al., 2010) and Na^+K^+ pump (Kanai et al., 2013). A rough surface of TM segments with a potential for acyl chain trapping can be found in virtually all available structures of membrane proteins (PDBTM database; Kozma et al., 2013). Whether there is any selectivity for particular lipids or fatty acids by the rough surface of helical TMDs remains to be evaluated. Experimental and *in silico* data (Pitman et al., 2005; Polozova and Litman, 2000) suggest the preference of polyunsaturated fatty acids for the annulus, a finding that is in agreement with a tendency of cells to keep membrane fluid even in the presence of rigidifying effects. Our results from the system containing PAPC, glycerophospholipid containing one saturated (palmitoyl; C16:0) and one polyunsaturated acyl chain (arachidonoyl; C20:4), indicate that the rough surface of proteins has a rigidifying effect even in membranes with unsaturated fatty acids and hybrid lipids. The inverse correlation between protein density and lateral diffusion previously observed in model and cell membranes, therefore, might not be exclusively explained by the impact of crowding (Ramadurai et al., 2009; Peters and Cherry, 1982; Frick et al., 2007). A majority of proteins in membranes are mobile and contain only a few TMDs that cannot be considered obstacles for small membrane components such as lipids. In this work, we show that integral proteins reduce the mobility of membrane lipids and proteins independent of their size or higher-order organization.

Our data also provide a likely explanation for the earlier findings that integral proteins and peptides prefer more fluid areas in phase-separated membranes (Schafer et al., 2011; Fastenberg et al., 2003). First, the rough surface of TM segments causes increased local viscosity. In more rigid membranes, this could cause significant reduction in the mobility of membrane molecules and, potentially, their immobilization. Moreover, highly unsaturated acyl chains of lipids were shown to preferentially associate with TMDs (Pitman et al., 2005; Polozova and Litman, 2000). Such lipids have a local disordering effect, thus preventing the immobilization of membrane molecules. In cells, immobilization of the components of signaling or metabolic pathways would be in conflict with the fact that these processes are largely driven by the diffusion of highly mobile molecules (e.g., in membranes; Cebecauer et al., 2010). Indeed, it seems that membrane proteins are sorted to more fluid parts of the membranes, thus avoiding their uncontrolled immobilization. Transiently immobilized surface receptors were shown to be rapidly eliminated from the plasma membrane by endocytosis (Andrews et al., 2008).

In ternary membranes, we demonstrate that the impact of the TM helical peptide on membrane dynamics is further escalated by the segregation of planar molecules like cholesterol from its rough surface (Figure 5). This, in principle, could lead to a segregation of the two molecules into different membrane domains. Indeed, reported electron microscopic images of plasma membrane sheets reproducibly indicate the coexistence of protein-rich and protein-low regions (Wilson et al., 2000). It remains to be determined whether cholesterol is predominantly found in one of those two regions of the plasma membrane. A tendency of cholesterol to segregate from TMDs might help the formation and/or stabilization of cholesterol-enriched, protein-low domains, a principle that was previously suggested in the literature (Nyholm, 2015).

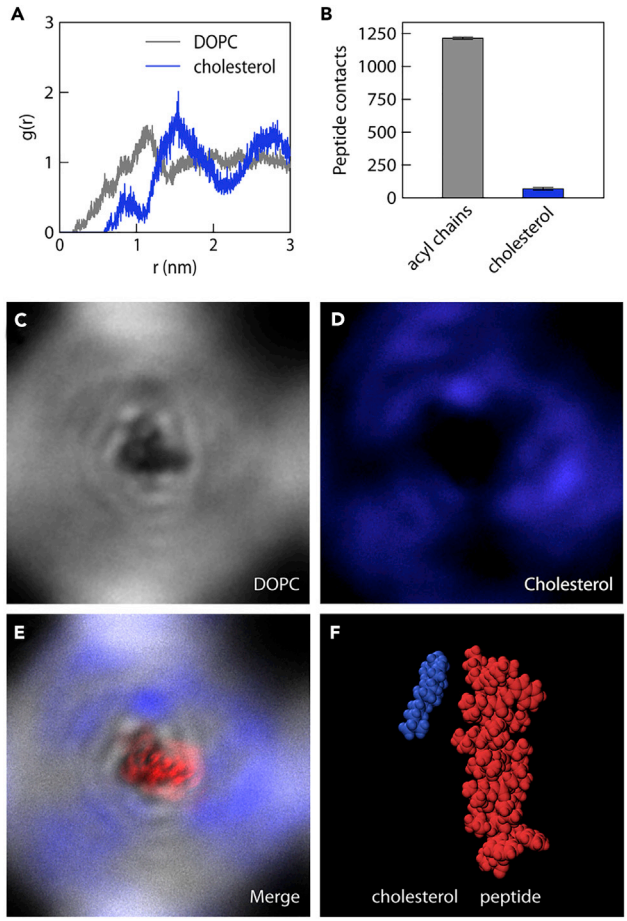

Figure 5. Cholesterol Segregation from the Rough Surface of the LW21 Peptide

(A) Pair correlation function [g(r)] of phospholipids and cholesterol from the center of mass of the peptide calculated in MD simulations of the LW21 peptide in a DOPC/cholesterol membrane (Video S2). The function quantifies the probability of intermolecular distances between the peptide and lipids with respect to those in an ideally mixed system. The molecular composition of the system characterized by the MD simulation is in Table S5.

(B) Quantification of phospholipid and cholesterol contacts with the peptide in a simulated membrane as in (A). Error bars represent error of the mean estimated by the block averaging method.

(C–E) Distribution maps of phospholipids (C) and cholesterol (D) in membrane containing the peptide. (E) The merged distribution map showing phospholipids in gray, cholesterol in blue and the peptide in red. The peptide was centered, and rotations were removed by data postprocessing.

(F) Cholesterol structure (blue) forms a planar interface that cannot fill the grooves on the surface of the LW21 peptide (red). Structures of both molecules are shown as van der Waals (ball) representations using VMD software. A typical snapshot from the MD trajectory is presented with one representative cholesterol molecule residing in the vicinity of the peptide. Remaining cholesterol molecules, phospholipids (DOPC), and water were removed for clarity.

The physical impact of the TMD roughness on membrane dynamics and organization demonstrated in this work may have other, previously unexpected consequences for membrane-associated processes in cells. Reduced lateral diffusion was observed in areas of the plasma membrane with higher protein density in living cells (Frick et al., 2007). This implies that reorganization of proteins, e.g., through interaction of ligands and cytoskeleton with receptors, might cause transient local reduction in the mobility of membrane molecules. Consequently, the slowdown of intermolecular interactions may positively or negatively affect the reaction kinetics of membrane-associated processes and thus affect the vital functions of living cells.

Limitations of Study

Some combinations of amino acids can form "less rough" surface of TM helices, and it would be interesting to know how peptides with different surface roughness influence membranes. However, the differences will

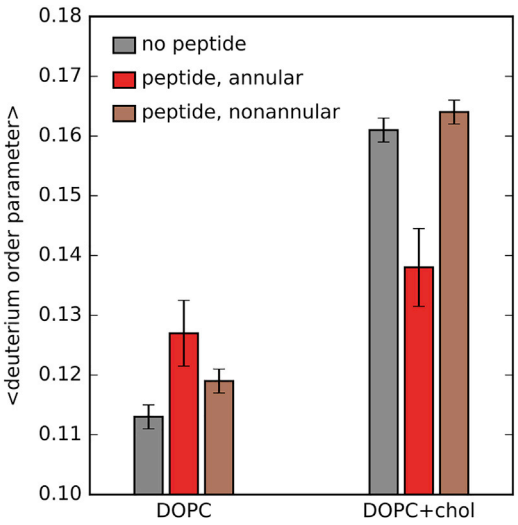

Figure 6. Acyl Chain Ordering in Membranes Containing the LW21 Peptide Was Calculated from MD Simulation Data

The graph represents the average deuterium order parameter S_{CD} of *sn*-2 acyl chains of DOPC in the absence (left) or presence (right) of 25 mol % cholesterol. Peptide-free membranes (gray bars) are compared with annular (red bars) and non-annular lipids (brown bars) of the LW21 peptide. Error bars represent error of the mean calculated based on the block averaging method. The ordering of acyl chains increases with S_{CD}. The acyl chain order parameter calculated from the angles between C-C bonds in the lipid acyl chain and the membrane normal (MD simulations) directly reflects the geometry of the acyl chain rather than its freedom to move. See also Table S4.

be always minute (e.g., for a peptide with alternating leucines and alanines), and we are confident that the available methods do not have sensitivity to distinguish between the changes caused by such peptides. Moreover, a poly-alanine peptide, which would represent probably the smoothest model helical peptide, does not stably incorporate into membranes in transbilayer orientation.

METHODS

All methods can be found in the accompanying Transparent Methods supplemental file.

SUPPLEMENTAL INFORMATION

Supplemental Information includes Transparent Methods, 10 figures, 5 tables, and 3 videos and can be found with this article online at https://doi.org/10.1016/j.isci.2018.11.026.

ACKNOWLEDGEMENTS

We would like to thank Anthony I. Magee for inspiring this project, Mariana Amaro and Silke Kerruth for their critical reading of the manuscript, Matti Javanainen for his comments on lipid diffusion analysis in the MD simulations, and Peter Kapusta for technical assistance. This work was funded by the Czech Science Foundation (M.C.: P305-11-0459, P208/12/G016; L.C.: 18-26751S). M.C. would like to acknowledge the Purkyne Fellowship and M.H. Praemium Academiae Award, both from the Czech Academy of Sciences. L.C. acknowledges the support from NF Neuron. Calculations were performed using National Grid Infrastructure MetaCentrum ("Projects of Projects of Large Research, Development, and Innovations Infrastructures," CESNET LM2015042).

AUTHOR CONTRIBUTIONS

M.O. and M.C. conceived the project; M.O., P.J., J. Sýkora, L.C., and M.H. designed the experiments; M.O., P.J., I.K., J. Sabó, and L.C. performed the experiments; and M.O., P.J., L.C., and M.C. wrote and edited the paper.

DECLARATION OF INTERESTS

The authors declare no competing interests.

Received: January 23, 2018
Revised: October 23, 2018
Accepted: November 14, 2018
Published: December 21, 2018

REFERENCES

Anderson, R.G., and Jacobson, K. (2002). A role for lipid shells in targeting proteins to caveolae, rafts, and other lipid domains. Science *296*, 1821–1825.

Andrews, N.L., Lidke, K.A., Pfeiffer, J.R., Burns, A.R., Wilson, B.S., Oliver, J.M., and Lidke, D.S. (2008). Actin restricts FcεRI diffusion and facilitates antigen-induced receptor immobilization. Nat. Cell Biol. *10*, 955–963.

Benda, A., Benes, M., Marecek, V., Lhotsky, A., Hermens, W.T., and Hof, M. (2003). How to determine diffusion coefficients in planar phospholipid systems by confocal fluorescence correlation spectroscopy. Langmuir *19*, 4120–4126.

Bernardino de la Sern, A.J., Schutz, G.J., Eggeling, C., and Cebecauer, M. (2016). There is no simple model of the plasma membrane organization. Front. Cell Dev. Biol. *4*, 106.

Bienvenue, A., Bloom, M., Davis, J.H., and Devaux, P.F. (1982). Evidence for protein-associated lipids from deuterium nuclear magnetic-resonance studies of rhodopsin-dimyristoylphosphatidylcholine recombinants. J. Biol. Chem. *257*, 3032–3038.

Brocchieri, L., and Karlin, S. (2005). Protein length in eukaryotic and prokaryotic proteomes. Nucleic Acids Res. *33*, 3390–3400.

Brotherus, J.R., Griffith, O.H., Brotherus, M.O., Jost, P.C., Silvius, J.R., and Hokin, L.E. (1981). Lipid-protein multiple binding equilibria in membranes. Biochemistry *20*, 5261–5267.

Camley, B.A., Esposito, C., Baumgart, T., and Brown, F.L. (2010). Lipid bilayer domain fluctuations as a probe of membrane viscosity. Biophys. J. *99*, L44–L46.

Cebecauer, M., Spitaler, M., Serge, A., and Magee, A.I. (2010). Signalling complexes and clusters: functional advantages and methodological hurdles. J. Cell Sci. *123*, 309–320.

de Planque, M.R., Greathouse, D.V., Koeppe, R.E., 2nd, Schafer, H., Marsh, D., and Killian, J.A. (1998). Influence of lipid/peptide hydrophobic mismatch on the thickness of diacylphosphatidylcholine bilayers. A ^{2}H NMR and ESR study using designed transmembrane alpha-helical peptides and gramicidin A. Biochemistry *37*, 9333–9345.

de Planque, M.R., and Killian, J.A. (2003). Protein-lipid interactions studied with designed transmembrane peptides: role of hydrophobic matching and interfacial anchoring. Mol. Membr. Biol. *20*, 271–284.

de Planque, M.R.R., Kruijtzer, J.A.W., Liskamp, R.M.J., Marsh, D., Greathouse, D.V., Koeppe, R.E., de Kruijff, B., and Killian, J.A. (1999). Different membrane anchoring positions of tryptophan and lysine in synthetic transmembrane α-helical peptides. J. Biol. Chem. *274*, 20839–20846.

Dupuy, A.D., and Engelman, D.M. (2008). Protein area occupancy at the center of the red blood cell membrane. Proc. Natl. Acad. Sci. U S A *105*, 2848–2852.

Fastenberg, M.E., Shogomori, H., Xu, X., Brown, D.A., and London, E. (2003). Exclusion of a transmembrane-type peptide from ordered-lipid domains (rafts) detected by fluorescence quenching: extension of quenching analysis to account for the effects of domain size and domain boundaries. Biochemistry *42*, 12376–12390.

Frick, M., Schmidt, K., and Nichols, B.J. (2007). Modulation of lateral diffusion in the plasma membrane by protein density. Curr. Biol. *17*, 462–467.

Gallova, J., Uhrikova, D., Hanulova, M., Teixeira, J., and Balgavy, P. (2004). Bilayer thickness in unilamellar extruded 1,2-dimyristoleoyl and 1,2-dierucoyl phosphatidylcholine vesicles: SANS contrast variation study of cholesterol effect. Colloids Surf. B Biointerfaces *38*, 11–14.

Harayama, T., and Riezman, H. (2018). Understanding the diversity of membrane lipid composition. Nat. Rev. Mol. Cell Biol. *19*, 281–296.

Heberle, F.A., and Feigenson, G.W. (2011). Phase separation in lipid membranes. Cold Spring Harb. Perspect. Biol. *3*, 1–13.

Hite, R.K., Li, Z., and Walz, T. (2010). Principles of membrane protein interactions with annular lipids deduced from aquaporin-0 2D crystals. EMBO J. *29*, 1652–1658.

Jacobson, K., Ishihara, A., and Inman, R. (1987). Lateral diffusion of proteins in membranes. Annu. Rev. Physiol. *49*, 163–175.

Jost, P.C., Griffith, O.H., Capaldi, R.A., and Vanderkooi, G. (1973). Evidence for boundary lipid in membranes. Proc. Natl. Acad. Sci. U S A *70*, 480–484.

Jost, P.C., Nadakavukaren, K.K., and Griffith, O.H. (1977). Phosphatidylcholine exchange between the boundary lipid and bilayer domains in cytochrome oxidase containing membranes. Biochemistry *16*, 3110–3114.

Kaiser, H.J., Orlowski, A., Rog, T., Nyholm, T.K., Chai, W., Feizi, T., Lingwood, D., Vattulainen, I., and Simons, K. (2011). Lateral sorting in model membranes by cholesterol-mediated hydrophobic matching. Proc. Natl. Acad. Sci. U S A *108*, 16628–16633.

Kanai, R., Ogawa, H., Vilsen, B., Cornelius, F., and Toyoshima, C. (2013). Crystal structure of a Na+-bound Na+,K+-ATPase preceding the E1P state. Nature *502*, 201–206.

Kozma, D., Simon, I., and Tusnady, G.E. (2013). PDBTM: protein Data Bank of transmembrane proteins after 8 years. Nucleic Acids Res. *41*, D524–D529.

London, E., and Feigenson, G. (1981). Fluorescence quenching in model membranes. An analysis of the local phospholipid environment of diphenylhexatrien and Gramicidin A. Biochim. Biophys. Acta *649*, 89–97.

Machan, R., Jurkiewicz, P., Olzynska, A., Olsinova, M., Cebecauer, M., Marquette, A., Bechinger, B., and Hof, M. (2014). Peripheral and integral membrane binding of peptides characterized by time-dependent fluorescence shifts: focus on antimicrobial peptide LAH(4). Langmuir *30*, 6171–6179.

Marsh, D. (2008). Protein modulation of lipids, and vice-versa, in membranes. Biochim. Biophys. Acta *1778*, 1545–1575.

Mouritsen, O.G., and Bloom, M. (1984). Mattress model of lipid-protein interactions in membranes. Biophys. J. *46*, 141–153.

Mouritsen, O.G., and Zuckermann, M.J. (2004). What's so special about cholesterol? Lipids *39*, 1101–1113.

Niemela, P.S., Miettinen, M.S., Monticelli, L., Hammaren, H., Bjelkmar, P., Murtola, T., Lindahl, E., and Vattulainen, I. (2010). Membrane proteins diffuse as dynamic complexes with lipids. J. Am. Chem. Soc. *132*, 7574–7575.

Nyholm, T.K. (2015). Lipid-protein interplay and lateral organization in biomembranes. Chem. Phys. Lipids *189*, 48–55.

Nystrom, J.H., Lonnfors, M., and Nyholm, T.K. (2010). Transmembrane peptides influence the affinity of sterols for phospholipid bilayers. Biophys. J. *99*, 526–533.

Oppenheimer, N., and Diamant, H. (2011). In-plane dynamics of membranes with immobile inclusions. Phys. Rev. Lett. *107*, 258102.

Peters, R., and Cherry, R.J. (1982). Lateral and rotational diffusion of bacteriorhodopsin in lipid bilayers: experimental test of the Saffman-Delbruck equations. Proc. Natl. Acad. Sci. U S A *79*, 4317–4321.

Pieper, U., Schlessinger, A., Kloppmann, E., Chang, G.A., Chou, J.J., Dumont, M.E., Fox, B.G., Fromme, P., Hendrickson, W.A., Malkowski, M.G., et al. (2013). Coordinating the impact of structural genomics on the human alpha-helical transmembrane proteome. Nat. Struct. Mol. Biol. *20*, 135–138.

Pitman, M.C., Grossfield, A., Suits, F., and Feller, S.E. (2005). Role of cholesterol and polyunsaturated chains in lipid-protein interactions: molecular dynamics simulation of rhodopsin in a realistic membrane environment. J. Am. Chem. Soc. *127*, 4576–4577.

Polozova, A., and Litman, B.J. (2000). Cholesterol dependent recruitment of di22:6-PC by a G protein-coupled receptor into lateral domains. Biophys. J. *79*, 2632–2643.

Raffy, S., and Teissie, J. (1999). Control of lipid membrane stability by cholesterol content. Biophys. J. *76*, 2072–2080.

Ramadurai, S., Duurkens, R., Krasnikov, V.V., and Poolman, B. (2010a). Lateral diffusion of membrane proteins: consequences of hydrophobic mismatch and lipid composition. Biophys. J. *99*, 1482–1489.

Ramadurai, S., Holt, A., Krasnikov, V., van den Bogaart, G., Killian, J.A., and Poolman, B. (2009). Lateral diffusion of membrane proteins. J. Am. Chem. Soc. *131*, 12650–12656.

Ramadurai, S., Holt, A., Schafer, L.V., Krasnikov, V.V., Rijkers, D.T., Marrink, S.J., Killian, J.A., and

Poolman, B. (2010b). Influence of hydrophobic mismatch and amino acid composition on the lateral diffusion of transmembrane peptides. Biophys. J. *99*, 1447–1454.

Rog, T., Murzyn, K., Karttunen, M., and Pasenkiewicz-Gierula, M. (2008). Nonpolar interactions between trans-membrane helical EGF peptide and phosphatidylcholines, sphingomyelins and cholesterol. Molecular dynamics simulation studies. J. Pept. Sci. *14*, 374–382.

Rog, T., Pasenkiewicz-Gierula, M., Vattulainen, I., and Karttunen, M. (2007). What happens if cholesterol is made smoother: importance of methyl substituents in cholesterol ring structure on phosphatidylcholine-sterol interaction. Biophys. J. *92*, 3346–3357.

Saffman, P.G., and Delbruck, M. (1975). Brownian motion in biological membranes. Proc. Natl. Acad. Sci. U S A *72*, 3111–3113.

Saxton, M.J. (1987). Lateral diffusion in an archipelago. The effect of mobile obstacles. Biophys. J. *52*, 989–997.

Schafer, L.V., de Jong, D.H., Holt, A., Rzepiela, A.J., de Vries, A.H., Poolman, B., Killian, J.A., and Marrink, S.J. (2011). Lipid packing drives the segregation of transmembrane helices into disordered lipid domains in model membranes. Proc. Natl. Acad. Sci. U S A *108*, 1343–1348.

Shezad, K., Zhang, K., Hussain, M., Dong, H., He, C., Gong, X., Xie, X., Zhu, J., and Shen, L. (2016). Surface roughness modulates diffusion and fibrillation of amyloid-beta peptide. Langmuir *32*, 8238–8244.

Sparr, E., Ash, W.L., Nazarov, P.V., Rijkers, D.T., Hemminga, M.A., Tieleman, D.P., and Killian, J.A. (2005). Self-association of transmembrane alpha-helices in model membranes: importance of helix orientation and role of hydrophobic mismatch. J. Biol. Chem. *280*, 39324–39331.

Stefl, M., Sachl, R., Humpolickova, J., Cebecauer, M., Machan, R., Kolarova, M., Johansson, L.B.A., and Hof, M. (2012). Dynamics and size of cross-linking-induced lipid nanodomains in model membranes. Biophys. J. *102*, 2104–2113.

van Meer, G., Voelker, D.R., and Feigenson, G.W. (2008). Membrane lipids: where they are and how they behave. Nat. Rev. Mol. Cell Biol. *9*, 112–124.

Wang, D., He, C., Stoykovich, M.P., and Schwartz, D.K. (2015). Nanoscale topography influences polymer surface diffusion. ACS Nano *9*, 1656–1664.

Weiss, K., Neef, A., Van, Q., Kramer, S., Gregor, I., and Enderlein, J. (2013). Quantifying the diffusion of membrane proteins and peptides in black lipid membranes with 2-focus fluorescence correlation spectroscopy. Biophys. J. *105*, 455–462.

Wilson, B.S., Pfeiffer, J.R., and Oliver, J.M. (2000). Observing FcεRI signaling from the inside of the mast cell membrane. J. Cell Biol. *149*, 1131–1142.

ISCI, Volume *10*

Supplemental Information

Roughness of Transmembrane Helices

Reduces Lipid Membrane Dynamics

Marie Olšinová, Piotr Jurkiewicz, Iryna Kishko, Jan Sýkora, Ján Sabó, Martin Hof, Lukasz Cwiklik, and Marek Cebecauer

Supplemental Figures

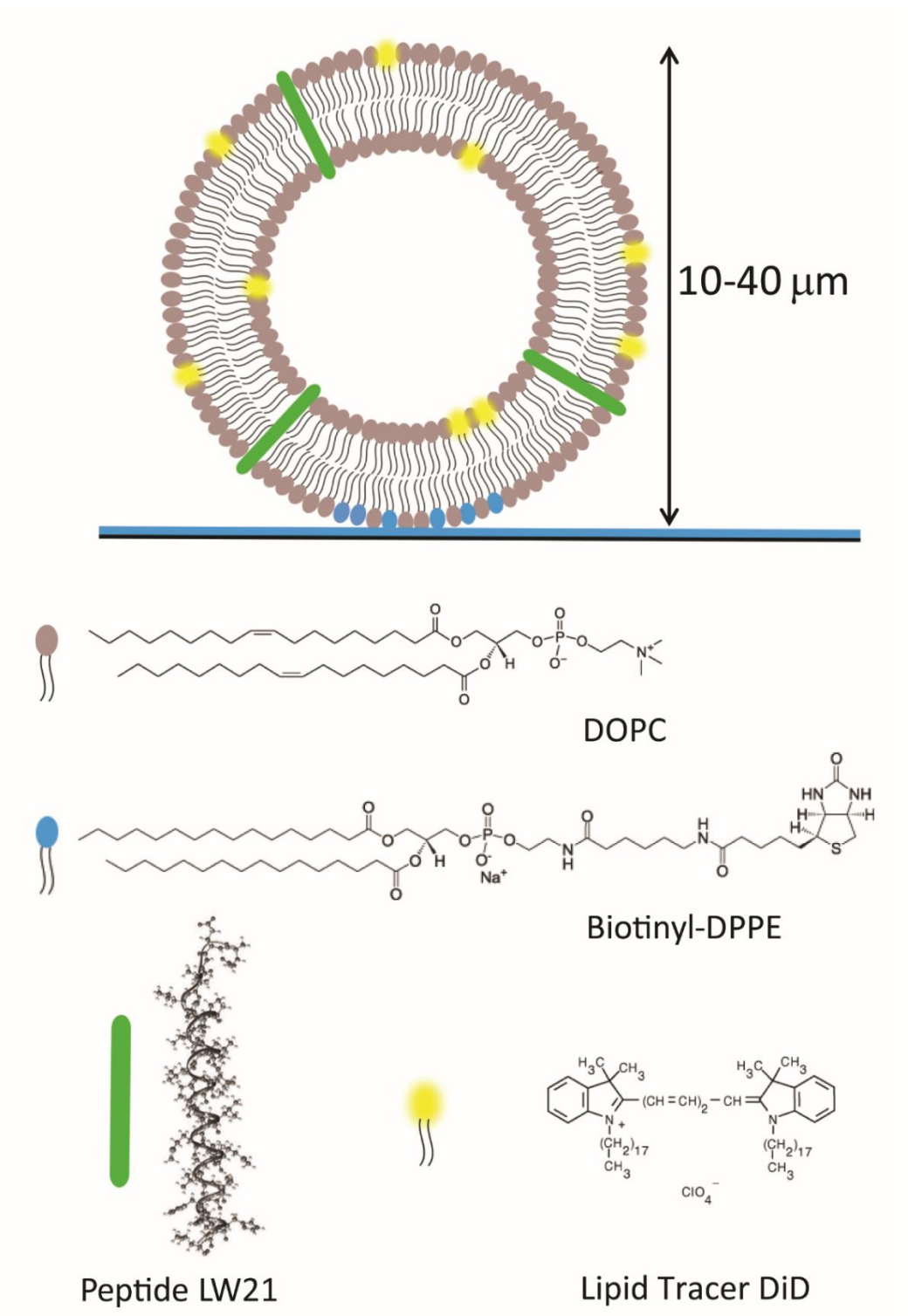

Figure S1, related to Figure 1A. Model membrane system. Schematic illustration of the model membrane system used in the experimental part of the work. Giant unilamellar vesicles (GUVs) containing DOPC (grey), lipid tracer (DiD; yellow) and LW21 peptides (green, amino acid sequence: **GLLDSKKWWLLLLLLLALLLLLLLLWWKKFSRS**) were attached to the optical surface via surface streptavidin binding to biotinylated lipids (blue) present in the membranes.

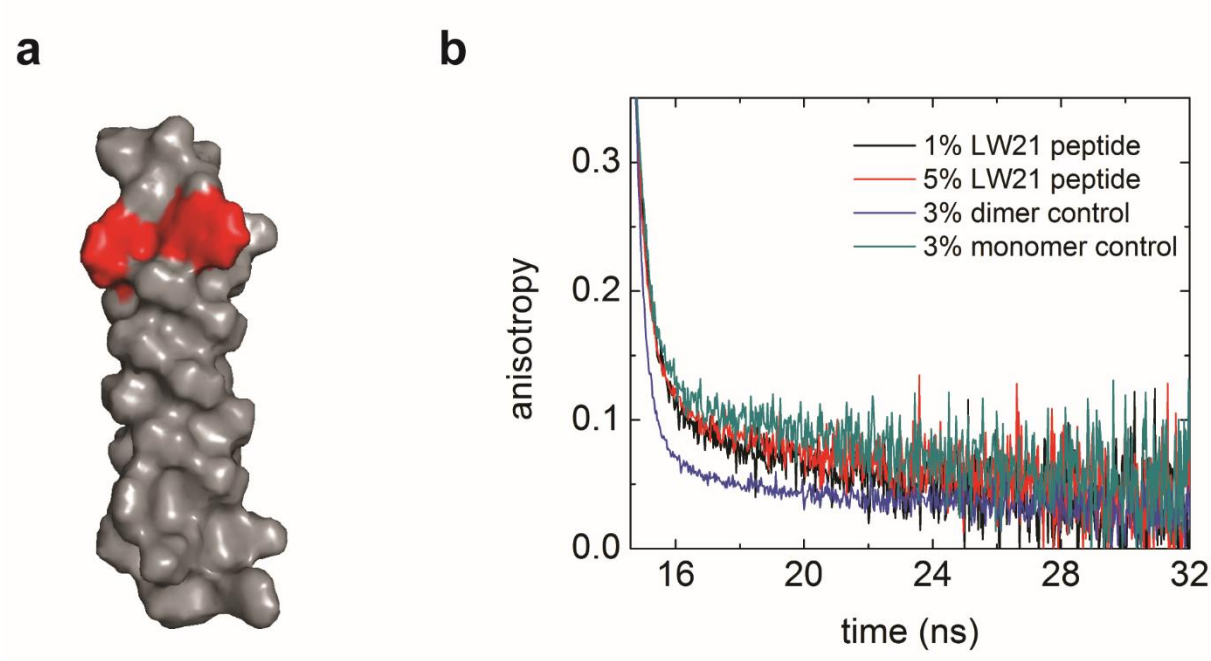

Figure S2, related to Figure 1A. LW21 peptide is monomeric and non-aggregated in tested membranes. a. Model of LW21 peptide with labelled tryptophan residues, which were used to investigate the oligomerization state of LW21 peptide in DOPC membranes (as in b). **b**. Time resolved fluorescence anisotropy decays of LW21, C_2-LW21 and melittin peptides in DOPC membranes demonstrate the monomeric state of LW21 peptide at both concentrations, 1 and 5 mol%. Melittin represents a monomeric control, whereas C_2-LW21 dimerizes due to the presence of free cysteine in its N terminus (see Chemicals and peptides in the Transparent Methods).

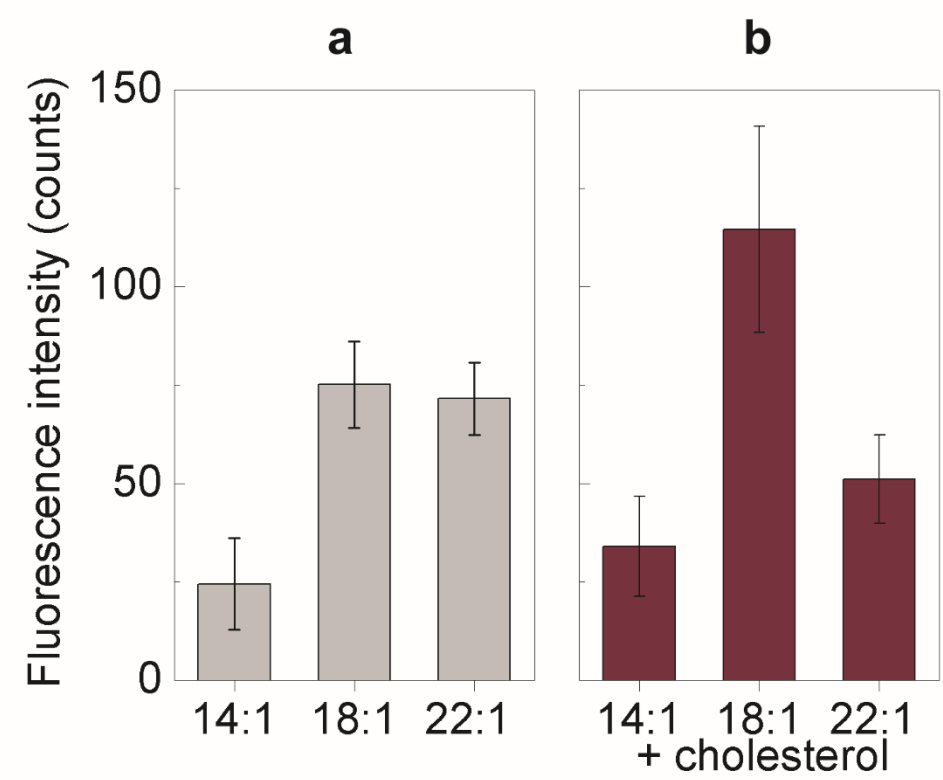

Figure S3, related to Figure 1A. The incorporation of the LW21 peptide into membranes composed of lipids with different thickness – acyl chain length – in the absence (**a**) or presence (**b**) of 25 mol% cholesterol. The values were calculated as the average fluorescence intensity measured for the fluorescent LW21 peptide (see Transparent Methods for more detail). Error bars indicate standard deviations (SD).

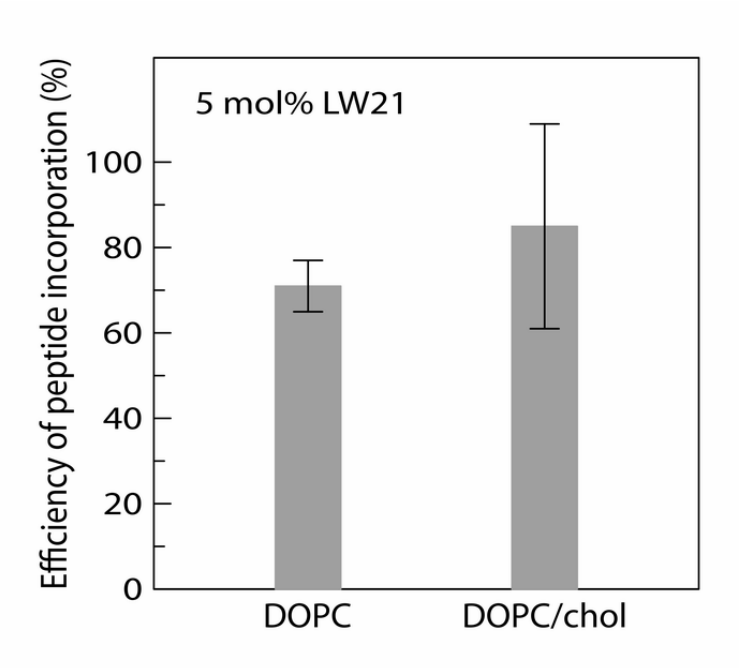

Figure S4, related to Figure 1A. Efficient incorporation of the LW21 peptide into LUVs composed of DOPC and DOPC:cholesterol (3:1). The LW21 peptides were first purified on C18 trap column by loading of vesicles solubilized in 10% ACN/1% formic acid in water and extensive washing with dichloromethane containing 1% formic acid. After elution, peptides were analyzed using semi-quantitative LC-MS method as described in Transparent Methods. Dry samples containing peptides (5 mol%) mixed with lipids, further analyzed identically as vesicles, were used as controls (= 100%). Relative peptide incorporation efficiency (%) is presented for membranes composed of DOPC and DOPC:cholesterol (3:1). Error bars represent standard deviation from at least 4 vesicle preparations.

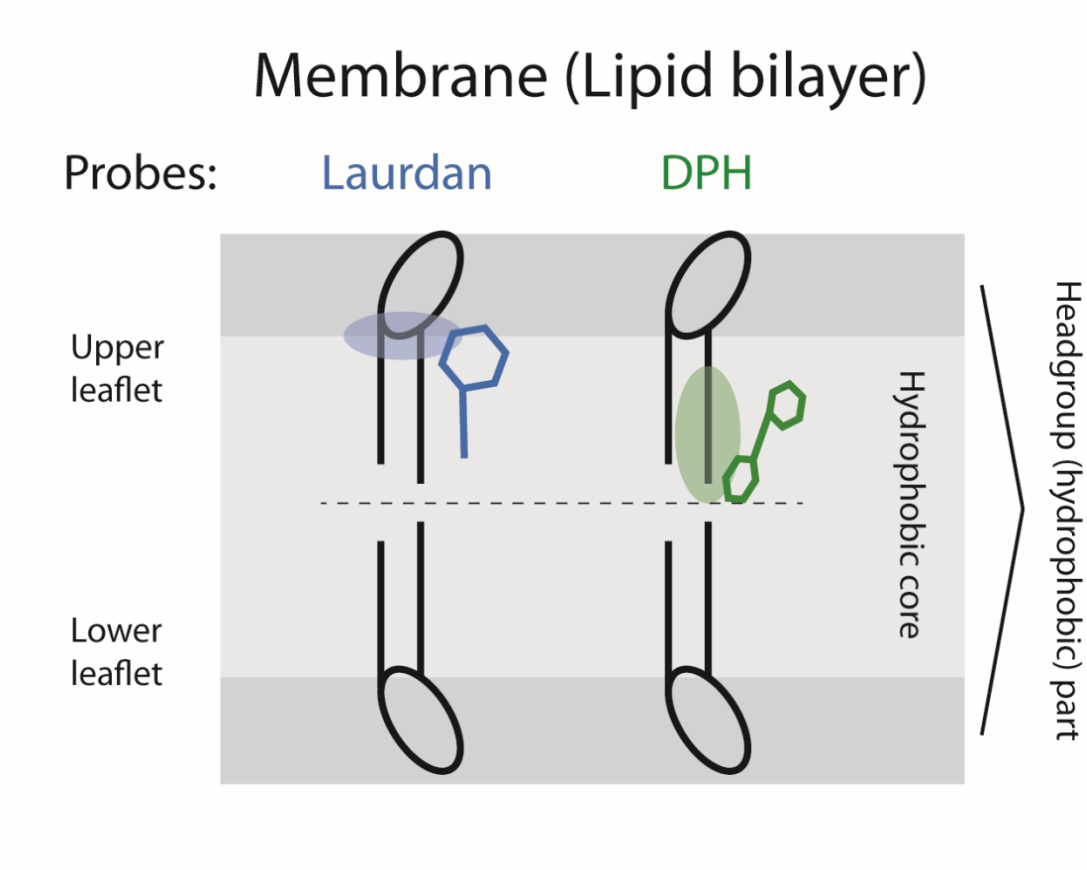

Figure S5, related to Figure 1B and Table 1. Schematic illustration of the membrane with environment-sensitive fluorescent probes Laurdan and DPH. Laurdan senses mobility and hydration at the level of phospholipid carbonyl groups (blue), DPH determines rotational freedom of acyl chains close to the center of lipid bilayer (green). In the experiments, both leaflets were labeled symmetrically.

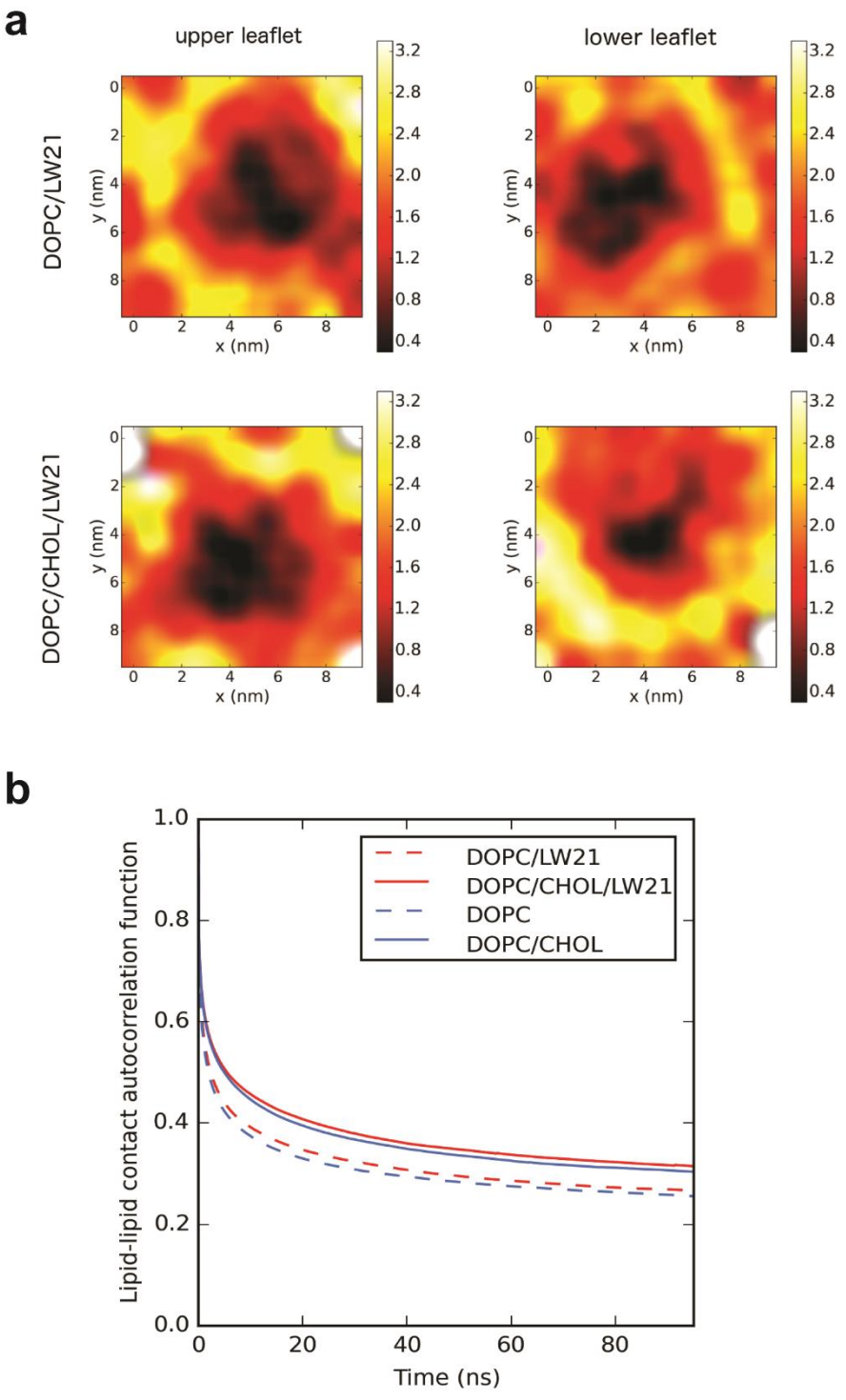

Figure S6, related to Figure 2. Retardation of phospholipids in the vicinity of the LW21 peptide surface – maps for all leaflets presented. a. Lateral diffusion maps of lipids as resolved by all-atom MD simulations in the absence (upper row) and presence of cholesterol (bottom row) for the individual membrane leaflets (left/right column). The maps are centered to an average position of the LW21 peptide. The plots show the average distance travelled by a lipid starting at a particular lateral position in a bilayer over 100 ns time. **b.** Lipid-lipid contact autocorrelation function calculated for DOPC and DOPC/cholesterol bilayers in the absence and presence of LW21 peptide. Contacts between acyl chain carbons were taken into account with the cut-off of 0.75 nm.

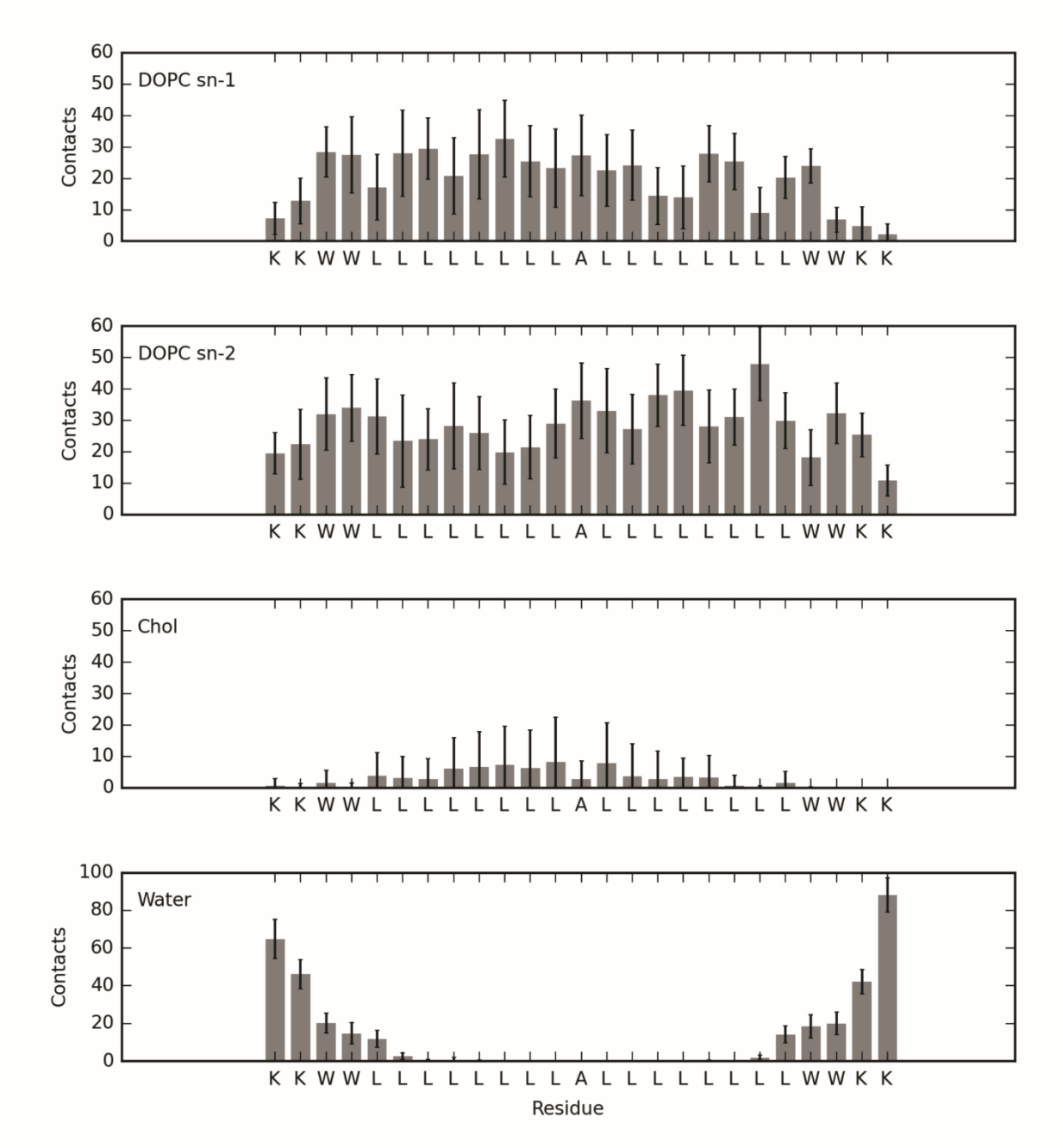

Figure S7, related to Figure 2. Quantitative analysis of contacts of DOPC, cholesterol and water with individual amino acids of the LW21 peptide. Average number of contacts between the peptide backbone and: *sn*-1 and *sn*-2 acyl chains of DOPC, cholesterol, and water per individual residues calculated from the MD simulation of LW21 in the DOPC membrane with 25 mol% of cholesterol. The cut-off value of 0.75 nm was employed for the contact definition. Error bars represent standard deviation. No specific interaction of lipids with individual amino acids is observed. The non-uniform contact distributions of both cholesterol (elevated close to the membrane mid-plane) and water (exclusively at the membrane-water interfaces) resemble the density profiles of these species in the membrane. Similarly, lower contact numbers between the peptide and acyl chains close to the peptide termini are due to decreased presence of lipid acyl chains therein.

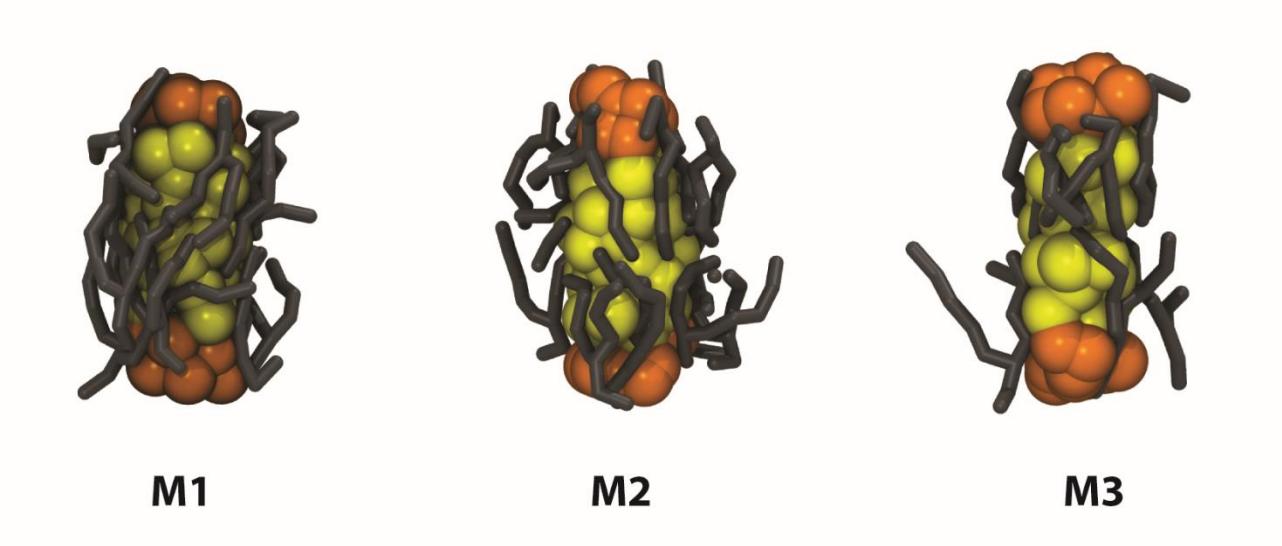

Figure S8, related to Fig. 4. The toy models of cylinder-like structures with annual lipids. The toy models M1-M3 (yellow-orange) were generated using coarse grain force field and embedded in DOPC lipid bilayer. The snapshots indicate lipids (grey), which have at least one MARTINI bead of their acyl chains within 0.5 nm distance from the surface of the toy models.

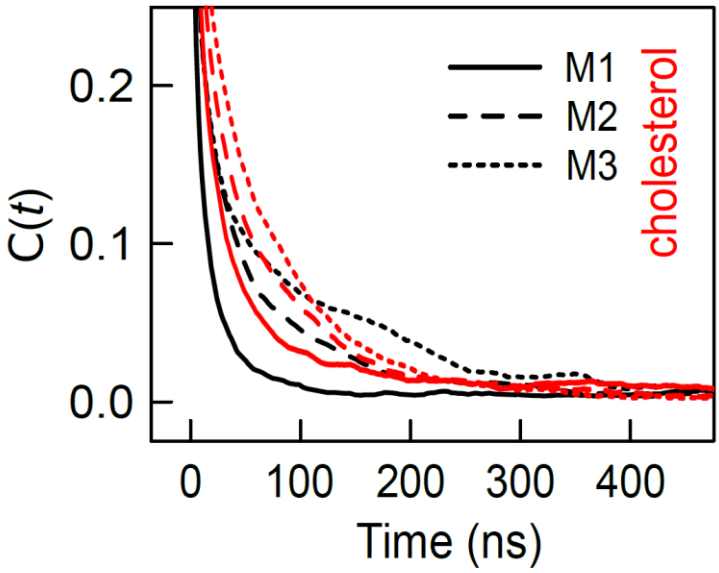

Figure S9, related to Fig 4. Cholesterol does not eliminate the effect of rough structures on lipid membrane dynamics. The autocorrelation curves for the contacts between lipid tails and the surface of model structures M1-M3 with increasing roughness (see Fig. 4a) embedded in DOPC membranes without (black) and with (red) cholesterol.

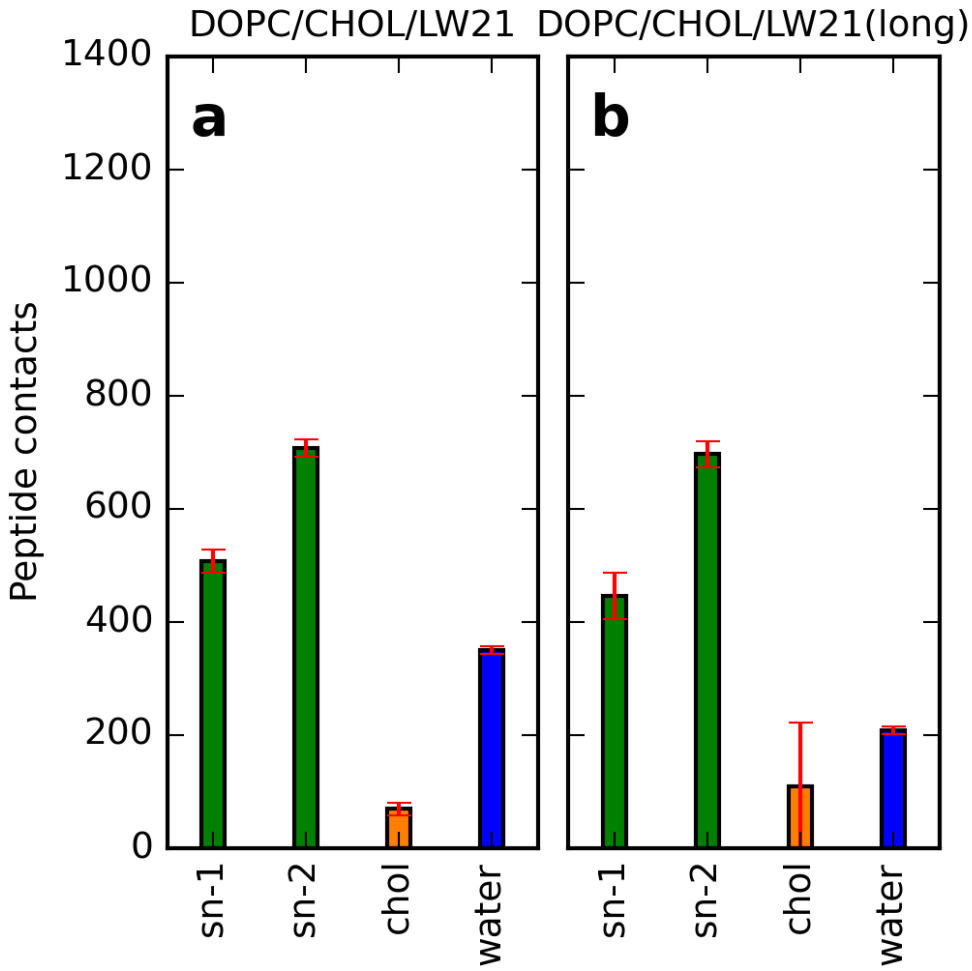

Figure S10, related to Figure 5. The LW21 flanking residues do not influence the contacts of DOPC, cholesterol and water with the peptide. The graphs present the average number of contacts formed by phospholipid acyl chains (*sn*-1 and *sn*-2), cholesterol and water with LW21 peptide backbone. Data for DOPC membranes containing 25 mol% cholesterol (membranes are shown for LW21 either without (**a**) and with (**b**) flanking residues. The results are virtually the same for both versions of the peptide (GLLDSKKWWLLLLLLLALLLLLLLWWKKFSRS; short version underlined). The data show negligible impact of flanking residues on lipid-peptide contacts. Error bars represent error of the mean calculated employing the block averaging method.

Supplemental Tables

Table S1, related to Figure 1A. Average anomalous coefficients and standard deviations calculated for lipid marker (DiD) dye in membranes with and without cholesterol. Anomalous coefficients were obtained by fitting of autocorrelation curves to a model of anomalous diffusion in 2D. Autocorrelation curves were calculated for the z-position where the membrane was in focus.

Peptide content [%]	Anomalous coefficient	
	DOPC	DOPC + chol
0	0.99 ± 0.02	0.99 ± 0.02
1	0.99 ± 0.01	0.99 ± 0.01
2	0.99 ± 0.01	0.99 ± 0.01
3	0.99 ± 0.01	0.99 ± 0.01

Table S2, related to Figure 1A. Ratio of diffusion coefficients with and without cholesterol for specific peptide content. Diffusion coefficients and standard deviations of fluorescently labelled peptides and lipid tracers measured by z-scan FCS method on top of GUVs.

Unlabelled LW21 peptide	$D_{Atto488LW21}$ [μm²/s]			D_{DiD} [μm²/s]		
	0% cholesterol	25% cholesterol	D_{25}/D_0	0% cholesterol	25% cholesterol	D_{25}/D_0
0%	10.5 ± 1.2	8.8 ± 1.1	0.8 ± 0.2	13.2 ± 0.5	9.1 ± 1.3	0.7 ± 0.1
1%	8.3 ± 0.6	7.8 ± 1.2	0.9 ± 0.2	11.3 ± 0.9	8.6 ± 0.8	0.8 ± 0.1
2%	7.5 ± 1.2	5.5 ± 1.4	0.7 ± 0.3	10.1 ± 1.1	6.3 ± 1.8	0.6 ± 0.3
3%	6.6 ± 1.3	2.9 ± 0.8	0.4 ± 0.2	8.8 ± 1.0	3.7 ± 1.1	0.4 ± 0.2

Table S3, related to Figure 1B. Total spectral shift Δν of Laurdan embedded in LUVs composed of either pure DOPC or DOPC:Chol (3:1, molar ratio) measured at 25°C. Total spectral shift is directly proportional to the polarity of the dye environment. Error bars give intrinsic uncertainty of the method.

Content of unlabeled LW21 peptide (mol%)	**$\Delta\nu_{DOPC}$ (cm^{-1})**	**$\Delta\nu_{DOPC+cholesterol}$ (cm^{-1})**
0	4080 ± 50	4160 ± 50
1	4080 ± 50	4140 ± 50
2	4100 ± 50	4140 ± 50
3	4070 ± 50	4090 ± 50

Table S4, related to Figure 6. Acyl chain deuterium order parameter S_{CD} (MD simulations).

System	**<order parameter> S_{CD}**	**error**
DOPC	0.113	0.004
DOPC/LW21 annular	0.127	0.011

DOPC/LW21 non-annular	0.119	0.004
DOPC/CHOL	0.161	0.004
DOPC/CHOL/LW21 annular	0.138	0.013
DOPC/CHOL/LW21 non-annular	0.164	0.004

Table S5, related to Figures 2 and 5. Composition of the systems characterized using fully atomistic MD simulations. Each bilayer was hydrated with ~6700 water molecules. Four Cl^- counterions were added in the case of LW21-containing bilayers to neutralize the system.

System	**# lipids**	**# cholesterol**	**# LW21**
DOPC	128	0	0
DOPC/CHOL	128	40	0
DOPC/LW21	128	0	1
DOPC/CHOL/LW21	128	40	1
DOPC/CHOL/LW21(long)	128	40	1

Transparent Methods

Chemicals and peptides

All chemicals and organic solvents were purchased from Sigma-Aldrich and Merck, or otherwise stated. Lipids 1,2-dimyristelaidoyl-*sn*-glycero-3-phosphocholine (14:1 PC, IUPAC name: [(2R)-2,3-bis[[(Z)-tetradec-9-enoyl]oxy]propyl] 2-(trimethylazaniumyl)ethyl phosphate), 1,2-dioleoyl-*sn*-glycero-3-phosphocholine (DOPC; 18:1 PC, IUPAC name: [(2R)-2,3-bis[[(Z)-octadec-9-enoyl]oxy]propyl] 2-(trimethylazaniumyl)ethyl phosphate), 1,2-dierucoyl-*sn*-glycero-3-phosphocholine (22:1 PC, IUPAC name: [(2R)-2,3-bis[[(Z)-docos-13-enoyl]oxy]propyl] 2-(trimethylazaniumyl)ethyl phosphate), 1-palmitoyl-2-arachidonoyl-*sn*-glycero-3-phosphocholine (PAPC, 16:0-20:4 PC, IUPAC name: 2-[[(2R)-3-hexadecanoyloxy-2-[(5Z,8Z,11Z,14Z)-icosa-5,8,11,14-tetraenoyl]oxypropoxy]-hydroxyphosphoryl]oxyethyl-trimethylazanium), 1,2-dipalmitoyl-sn-glycero-3-phosphoethanolamine-N-(cap biotinyl) (biotinylated-DPPE), 1,2-dioleoyl-*sn*-glycero-3-phosphoethanolamine (DOPE, IUPAC name: [(2R)-3-[2-aminoethoxy(hydroxy)phosphoryl]oxy-2-[(Z)-octadec-9-enoyl]oxypropyl] (Z)-octadec-9-enoate) and cholesterol (from ovine wool, IUPAC name: (3S,8S,9S,10R,13R,14S,17R)-10,13-dimethyl-17-[(2R)-6-methylheptan-2-yl]-2,3,4,7,8,9,11,12,14,15,16,17-dodecahydro-1H-cyclopenta[a]phenanthren-3-ol) were purchased from Avanti Polar Lipids, Inc. (Alabaster, AL, USA), streptavidin (IUPAC name: 2-[(3-chlorophenyl)-piperidin-1-ium-1-ylidenemethyl]sulfanylacetic acid) from IBA (Goettingen, Germany), and 2,2,2-trifluoroethanol (TFE) from Alfa Aesar (Karlsruhe, Germany). Fluorescent probes DiI.C_{18} (DiD, IUPAC name: 2-[5-(3,3-dimethyl-1-octadecylindol-1-ium-2-yl)penta-2,4-dienylidene]-3,3-dimethyl-1-octadecylindole;perchlorate) and 1,6-diphenyl-1,3,5-hexatriene (DPH, IUPAC name: [(1E,3E,5E)-6-phenylhexa-1,3,5-trienyl]benzene) were purchased from Sigma-Aldrich, 6-lauroyl-2-dimethylaminonaphthalene (Laurdan, IUPAC name: 1-[6-(dimethylamino)naphthalen-2-yl]dodecan-1-one) from Molecular Probes (Eugene, OR, USA), and Atto 488-maleimide from Atto-Tec (Siegen, Germany). Atto633-DOPE was prepared in our laboratory by coupling of Atto633 NHS ester (Atto-Tec) to the amine of DOPE followed by size-exclusion chromatography using P10 desalting column (GE Healthcare, Pittsburgh, PA).

Peptide LW21 (MW 4119, GLLDSKKWWLLLLLLLALLLLLLLLWWKKFSRS) and its fluorescently labelled variant Atto488-LW21 (MW 4933 Atto488-CGLLDSKKWWLLLLLLLALLLLLLLWWKKFSRS) were custom synthesized by VIDIA (Prague, Czech Republic). The identity and purity of the products (> 92%) were confirmed by mass spectrometry and analytical HPLC. The sequence of the LW21 peptide contains 21 hydrophobic residues flanked by two lysine residues of the original LW peptide (underlined; (Kaiser et al., 2011)) and a native sequence of the N- and C-terminal membrane proximal motifs from human CD247 (five N- and four C-terminal residues). We have added residues from CD247 molecule at both ends of the original LW21 peptide (Kaiser et al., 2011) to stabilize its transbilayer orientation. A stable transbilayer orientation of a peptide is important for our study since partial or peripheral association of the peptide with membranes could affect the experiments and reduce validity of the measurements. All atom MD simulations suggest minimal impact of flanking residues on herein studied effect of the rough surface of LW21 on membrane lipids (Figure S10). Solutions of 100 µM LW21, 100 µM C_2-LW21 and 1 µM Atto488-LW21 peptides were freshly prepared in TFE for each experiment. Dimeric peptide C_2-LW21 (MW 8579, (**C**GLLDPKKWWLLLLLLLALLLLLLLWWKKFSRS)$_2$; Biomatik, Wilmington, USA) was obtained by cysteine oxidation of monomeric peptide. The efficiency of dimerization (> 95%) was confirmed by mass spectrometry and HPLC. Synthetic melittin (MW 2845, GIGAVLKVLTTGLPALISWIKRKRQQ) was obtained from Sigma–Aldrich.

Preparation of model membranes (vesicles)

For vesicle preparation, lipids were dissolved in chloroform, fluorescent probes (DPH and Laurdan) in methanol and unlabeled LW21, C_2-LW21 and Atto488-LW21 peptides were dissolved in TFE.

LUV (large unilamellar vesicle) dispersion was prepared as described below. Lipids, peptide and fluorescent probes (probe:lipid molar ratio = 1:100) were mixed in the desired ratio in a glass tube. Organic solvents were evaporated under a stream of nitrogen while continuously incubated in a water bath (ambient temperature) and then kept under vacuum for at least 1 hour. The dry lipid film was hydrated in heated 105 mOsm/kg glucose buffer (40 °C, ~75 mM glucose, 10 mM HEPES, 10 mM NaCl and pH = 7.4) and vortexed for 5 minutes. The cycles of heating and vortexing were repeated until the lipids and peptides were completely suspended in the solution. To facilitate the detachment of peptides and lipids from the surface during the vortexing, glass beads (extensively cleaned; 2 mm in diameter) were added to the tube. LUVs were obtained by extrusion of lipid and peptide suspension through a polycarbonate membrane with an effective pore diameter of 100 nm (Avestin, Ottawa, Canada) by 50 passages at ambient temperature. Efficiency of peptides' incorporation into the lipid vesicles was verified by a semi-quantitative mass spectrometry analysis (see below). Monomeric control for anisotropy measurements was prepared by adding aqueous solution of melittin peptide which spontaneously integrates into lipid membranes, to the suspension of DOPC LUVs.

GUVs (giant unilamellar vesicles) were prepared by mixing lipids, peptides and probes in a desired ratio in a glass vial (2 ml) - altogether 100 nmol of all lipid species. For fluorescence correlation spectroscopy (FCS) experiments, GUVs contained DOPC, 0 or 25 mol% of cholesterol, 0-3 mol% of LW21 peptide and 2 mol% biotinylated-DPPE for the immobilization of vesicles at the BSA-biotin/streptavidin-coated glass coverslips. In addition, fluorescently labelled peptide Atto488-LW21 (peptide:lipid = 1:25 000, mol:mol) and lipid tracer, DiD (probe:lipid = 1:100 000, mol:mol), were added to lipid-peptide mixtures. For peptide incorporation studies, lipids of different acyl chain length were used (14:1 PC, 18:1 PC (DOPC), and 22:1 PC) and fluorescently labelled species were present in a higher content (Atto488-LW 1:1000, mol:mol, and fluorescent lipid, Atto633-DOPE, 1:20 000, mol:mol). Otherwise the composition was identical to the GUVs used for FCS. GUVs were prepared by electroformation according to Stockl and co-workers (Stockl and Herrmann, 2010). Briefly, lipids, peptides and fluorescent probes in organic solvents were spread on two preheated titanium slides. Slides were kept for 1 hour under vacuum to evaporate any residual solvent. The slides were then stuck together by melting Parafilm. The formed chamber was filled with 105 mOsm/kg sucrose in water and heated to 40°C. The process of vesicle formation was induced by applying a sinusoidal altering voltage (10 Hz) starting at 150 mV (peak-to-peak amplitude) and gradually increasing every 2.5 min with a step of 50 mV up to 1.1 V; this voltage was kept for another 90 minutes. At the end, a frequency of 4 Hz and voltage of 1.3 V were applied for 30 minutes for the detachment of vesicles. Prepared GUVs were transferred into a LabTek 8-well chamber slide (ThermoScientific, Waltham, USA) coated with BSA-biotin/streptavidin. Landing of GUVs on the optical surface was enabled by changing the buffer in the chamber for 105 mOsm/kg glucose (which has the same osmolality as sucrose buffer but lower density). Within one hour, GUVs were firmly attached to the coated glass surface and ready for imaging.

Determination of peptide incorporation efficiency by semi-quantitative mass spectrometry analysis of LUVs

The method for determination of peptide incorporation efficiency by semi-quantitative mass spectrometry was adapted from the previously published protocol (Vit et al., 2016). LUVs composed of DOPC or DOPC:cholesterol (3:1) with 5 mol% LW21 peptide were prepared as described above. Five aliquots, each containing 7.5 µg of the peptide in vesicles, were treated individually. For the control, peptides and lipids were mixed in a desired ratio in glass tubes. Organic solvents were evaporated under a stream of nitrogen while continuously incubated in a water bath (ambient temperature) and further kept under vacuum for at least 1 hour. The dry lipid/peptide film of control samples was further used without vesicle preparation and by application of the identical processes as for the samples with LUVs. For semi-quantitative analysis by liquid chromatography/mass spectrometry (LC/MS) technique, vesicles and lipid/peptides mixtures were first dissolved in 80% (v/v) acetonitrile (ACN) and 1 % (v/v) formic acid, then diluted eight-fold in 1 % (v/v) formic

acid and applied to the C18 trap column (OPTI-TRAP Micro, Peptide - Optimize Technologies, USA) for the removal of lipids from the samples. Columns were washed 3 times with 10% (v/v) ACN and 1% (v/v) formic acid in water to remove residual buffer and once with dichloromethane containing 1% (v/v) of formic acid to remove all traces of lipids. Peptides were eluted with 80% (v/v) ACN with 1% (v/v) of formic acid and dried using the speed-vac. Dried samples were first dissolved in trifluoroethanol followed by five-fold dilution in water containing 10% ACN with 0.1% of formic acid and applied to Agilent 1 200 HPLC system (Agilent Technologies, USA) for liquid chromatography separation on Zorbax SB-C18, 0,3x150 mm 3,5-micron column (Agilent Technologies). Samples were separated at constant temperature (50°C), at flow rate 10 µl/min and by linear gradient of solvent B (98% (v/v) ACN in 0.1% (v/v) aqueous formic acid) in solvent A (2% (v/v) ACN in 0.1% (v/v) aqueous formic acid) as follows: 0-3.5 min 30% B; 3.5-25 min ramping to 95% B; 25-29 min hold at 95% B; 29-30 min return to 30% B; 30-40 min equilibration at 30% B. ESI+ detection of ions was performed using 15T-solarix XR FT-ICR Mass Spectrometer (Bruker Daltonics, USA). For each aliquot, mass spectrum was acquired by calculating the area under chromatographic peak of the $[M+5H]^{5+}$ ion of the LW21 peptide. Other three dominant ion species could be recognized on a given spectrum: $[M+6H]^{6+}$, $[M+4H]^{4+}$ and $[M+3H]^{3+}$. Out of mentioned ion species, monoisotopic masses with the smallest m/z ratio were selected for quantification. The peptide incorporation efficiency (in %) was calculated as the amount of peptides in LUVs divided by the amount of peptides determined in control samples (Figure S4).

LUVs containing 5 mol% peptide were tested due to the sensitivity limitations of the method which led to a lower reproducibility of measurements when analyzing samples containing lower amount of the peptide (e.g. 1 mol%).

Determination of the peptide integration into GUVs

Peptide integration studies were performed on an inverted confocal fluorescence microscope Olympus X71 with the same optical setup as for FCS experiments. The intensity image of each GUV was acquired by scanning the XY plane cross-section in the middle of the vesicle with a pixel size of 100 nm. Several line profiles of fluorescence intensity were calculated for each GUV; two maximal values along every line profile were determined. The average of these values was used to compare the peptide integration in membranes composed of different lipids (14:1 PC, 18:1 PC (DOPC), and 22:1 PC). At least 12 vesicles for each membrane composition were analyzed.

Lateral mobility measurements – z-scan FCS

FCS measurements of GUVs were performed on an inverted confocal fluorescence microscope, Olympus IX71 (Olympus, Hamburg, Germany), equipped with single-photon counting unit MicroTime 200 (PicoQuant, Berlin, Germany). Excitation lasers of 470 and 635 nm (LDH-P-C-470 and LDH-D-C-635; PicoQuant), each with 10 MHz frequency, were used to illuminate a sample through the water-immersion objective (1.2 NA, 60x) (Olympus). The laser intensity measured at the sample position reached 5 µW and 0.5 µW for 470 nm and 635 nm lasers, respectively. The lasers were pulsing in alternating mode in order to avoid artefacts caused by signal bleed-through. Fluorescence signal was gathered through the main dichroic (Z473/635, Chroma, Rockingham, VT), 50 µm pinhole and guided to the emission dichroic mirror (620DCXR, Chroma) which splits the signal between the two single photon avalanche diodes using 515/50 and 685/50 band pass filters (Chroma). The measurements were performed at 25°C.

Lateral diffusion of membrane components was obtained by employing fluorescence correlation spectroscopy (FCS, for the details see ref. (Machan and Hof, 2010)). Autocorrelation function of the temporal fluorescence intensity fluctuations contains the information about the average number of particles *N* in the detection volume and characteristic time, τ_D, the molecule spends on average inside the detection volume (diffusion time). *N* and τ_D are obtained by fitting the autocorrelation function with *a priori* known model: eq.

1 for the lipid lateral mobility, eq. 2 for peptide lateral mobility. Eq. 2 takes into account the free dye not bound to the peptide (i.e. correction for the sample impurity originating from imperfect peptide labelling).

$$G_{2D}(\tau) = 1 + [1 - X + X \cdot exp(^{-\tau}/_{\tau_X})] \frac{1}{N(1-X)} \frac{1}{1+(^{\tau}/_{\tau_D})} \quad (1)$$

$$G_{3D2D}(\tau) = 1 + [1 - X + X \cdot exp(^{-\tau}/_{\tau_X})] \frac{1}{N(1-X)} \left(\frac{FR_{3D}}{1+(^{\tau}/_{\tau_{D_3}})} \frac{1}{\left(1+\frac{\tau}{\tau_{D_3}}\left(\frac{w_0}{w_z}\right)^2\right)^{\frac{1}{2}}} + \frac{1-FR_{3D}}{1+(^{\tau}/_{\tau_{D_2}})} \right) \quad (2)$$

The $G_{2D}(\tau)$ and $G_{3D2D}(\tau)$ are calculated autocorrelation functions for the delay time, τ, X is an average fraction of molecules in the dark state (due to intersystem crossing or cis/trans isomerization; typically set to zero for $G_{3D2D}(\tau)$), τ_X represents dark state relaxation time, FR_{3D} is a fraction of molecules moving in 3D space, τ_{D3} and τ_{D2} are characteristic diffusion times for molecules moving in 3D and 2D space, w_0 and w_z are the lateral and radial dimensions of the confocal volume, respectively, obtained as the distance from and along the optical axis at which the intensity drops to e^{-2}.

For the determination of anomalous diffusion of lipids, the anomalous exponent α is included in the fitting model of autocorrelation function. Considering the lipid lateral movement in membrane:

$$G_{2D,anomal}(\tau) = 1 + [1 - X + X \cdot exp(^{-\tau}/_{\tau_X})] \frac{1}{N(1-X)} \frac{1}{1+(^{\tau}/_{\tau_D})^{\alpha}} \quad (3)$$

where $\alpha = 1$ for free diffusion and $0 < \alpha < 1$ for anomalous diffusion.

To overcome the difficulties of precise volume determination for the conversion of τ_D determined by FCS to diffusion coefficient D, z-scan FCS variant was employed. *Z*-scan FCS represents a calibration-free method providing the diffusion coefficient and the radius of confocal volume in lateral plane (Benda et al., 2003). The z-scan FCS method is based on recording a set of measurements of the labelled membrane positioned differently in respect to the z-axis of the microscope. Intensity fluctuations are recorded in several consecutive z-positions separated by 200 nm with the top of GUV membrane placed ideally in the center of the *z*-stack. Analysis of calculated autocorrelation curves yields the set of τ_D. Fitting the parabolic dependence of τ_D on the position along the microscope *z*-axis provides directly the lateral diffusion coefficient D (eq. 4).

$$\tau_D = \frac{w_0^2}{4D}\left(1 + \frac{\lambda^2 \Delta z^2}{\pi n^2 w_0^4}\right), \quad (4)$$

where λ is the wavelength of the excitation light, Δz is the distance between the sample position z and the position of the beam diameter minimum z_0, and n is refractive index of the medium. Correlation functions were calculated and fitted to the described models (equations (1)-(4)) by in-house routine implemented in OriginPro 8 (OriginLab Corporation, Massachusetts, USA, http://www.originlab.com/). (Benda et al., 2003)

Time-resolved emission spectra of the Laurdan probe

Time resolved emission spectra (TRES) were obtained by spectral reconstruction from the recorded steady state emission spectra and time resolved fluorescence decays. Steady-state fluorescence emission spectra (λ_{EX} = 376 nm) were recorded for the dispersion of Laurdan-labelled LUVs with different peptide:lipid composition (lipid concentration: 1 mM) using Fluorolog-3 spectrofluorimeter (model FL3-11, JobinYvon Inc., Edison, NJ, USA) maintained at 25°C using a water-circulating thermostat. Fluorescence decays were collected by IBH 5000 U SPC equipment (Horiba Jobin Yvon) with a picosecond diode laser (IBH NanoLED-

375LH, peak wavelength 376 nm, 1 MHz repetition rate). Decays were recorded at series of wavelengths spanning the steady-state emission spectrum (400–540 nm) in 10 nm steps. To eliminate scattered light, a 399 nm cut-off filter was applied. The signal was kept below 2% of the light source repetition rate, and the data were collected in 8192 channels (0.014 ns per channel) until the peak value reached 5 000 counts. Fluorescence decays of Laurdan fluorescence were fitted by the three-exponential model of iterative re-convolution method using IBH DAS 6 software (IBH, UK). Parameters obtained from the fluorescence decay fits and steady state emission spectra were employed to reconstruct TRES by in-house routine implemented in Matlab. TRES were fitted with log-normal function to obtain the time evolution of their spectral maximum $\nu(t)$ (Horng et al., 1995). Two main parameters were derived from $\nu(t)$:

1) Overall emission shift $\Delta\nu$, which is directly proportional to the polarity of the dye microenvironment

$$\Delta\nu = \nu(0) - \nu(\infty) \quad (5)$$

where $\nu(0)$ = 23 800 cm^{-1} (estimated using method of Fee and Maroncelli; (Fee and Maroncelli, 1994)) and $\nu(\infty)$ stands for the position of the TRES emitted from the fully relaxed state.

2) Relaxation time τ_R, which provides a measure of the speed of dipolar relaxation. This parameter is inversely proportional to the mobility of the microenvironment of the dye. For Laurdan embedded in a lipid bilayer, τ_R reflects mobility of lipid moieties at the level of the carbonyl groups and peptide amino acid residues in the vicinity of the probe.

$$\tau_R = \int_0^\infty \frac{\nu(t) - \nu(\infty)}{\Delta\nu} dt. \quad (6)$$

Time-resolved fluorescence anisotropy

Fluorescence polarization experiments were performed using the same time resolved fluorescence spectrometer as for the TRES data. Measurements consisted of the recording of fluorescence decays with the 2 different orientations of the emission and excitation polarizers. The anisotropy decay r(t) was then calculated according to eq. (7):

$$r(t) = \frac{I_{VV}(t) - G \cdot I_{VH}(t)}{I_{VV}(t) + 2 \cdot G \cdot I_{VH}(t)} \quad (7)$$

where I_{VV} is the fluorescence decay measured with both excitation and emission light polarized vertically, and I_{VH} with the vertically polarized excitation and horizontally polarized emission light. G-factor (G) was determined by acquiring fluorescence decays for a standard solution of free dye (10 μM POPOP in ethanol or 40 μM tryptophan dissolved in PBS buffer) applying a tail matching method using FluoFit v.4.5 (PicoQuant). Anisotropy decay $r(t)$ was fitted with single exponential

$$r(t) = r_\infty + (r_0 - r_\infty) \exp\left(-t/\varphi\right), \quad (8)$$

where r_∞ is residual anisotropy, r_0 initial anisotropy, and φ rotational correlation time.

Specifically, the anisotropy decays were measured either for DPH probe embedded in the membrane or for the tryptophans of LW21 peptides incorporated in the membrane. For the former set of experiments, the DPH-labelled LUV dispersion (lipid concentration: 0.5 mM) was excited by the picosecond diode laser 376 nm (IBH NanoLED-375LH, peak wavelength 376 nm, 1 MHz repetition rate). The emission monochromator was set to 466 nm. A 399 nm cut-off filter was applied to eliminate scattered light. The difference between the maxima of I_{VV} and I_{VH} decays was set to 20000 counts. The anisotropy data were analyzed according to the "wobble in cone" model introduced by Kawato et al. (Kawato et al., 1977) and Kinosita et al. (Kinosita et al., 1982). The S-order parameter (S) was calculated according to eq. 9:

$$S = \sqrt{\frac{r_\infty}{r_0}}, \quad (9)$$

In the case of tryptophan anisotropy, dispersion of LUVs (0.5 mM lipid concentration) with indicated peptides was excited by 295 nm diode (Picoquant; PLS-8-2-257, 5 MHz repetition rate). The excitation light was guided through the polarizer directly into the sample and the emission monochromator was set to 350 nm. The difference between the maxima of I_{VV} and I_{VH} decays was set to 50000 counts. The data were collected in 4096 channels (0.028 ns per channel). The rate of Trp anisotropy decay determines the efficiency of the energy homo-transfer. A higher transfer efficiency is caused by the close proximity of the two helices (their tryptophan side chains), suggesting that a peptide forms dimers (or higher oligomers).

All-atom molecular dynamics (MD) simulations of the peptide in lipid membranes

Classical MD simulations were performed for five systems characterized in the Table S5. All systems were prepared based on previously equilibrated DOPC and cholesterol bilayer consisting of 128 DOPC (64 in each leaflet) and 40 cholesterol molecules hydrated with approximately ~6700 water molecules. LW21 peptide molecule (KKWWLLLLLLLLALLLLLLLLWWKK) was incorporated both in pure DOPC and DOPC with cholesterol membranes in the transbilayer orientation employing a variant of the method advised by Javanainen and Martinez-Seara (Javanainen and Martinez-Seara, 2016). For comparison, the system (DOPC/CHOL/LW21(long)) containing DOPC, cholesterol, and a variant of LW21 with extra flanking residues (GLLDSKKWWLLLLLLLALLLLLLLLWWKKFSRS; the peptide used for the experimental procedures) was also simulated (Figure S10). The LW21 molecule was prepared based on an ideally helical structure employing the `pdb2gmx` tool from the Gromacs software package (Hess et al., 2008). The Amber03 force field was employed for the peptide (Sorin and Pande, 2005). Lipid molecules were described using the `Slipids` force field (Jambeck and Lyubartsev, 2012) while the `TIP3P` model was employed for water (Vega and de Miguel, 2007). Note that the recently developed `Slipids` force field was designed to be compatible with the `Amber` parameterization. Each system was simulated employing a rectangular prismatic shape simulation box of the size of approximately 6.8 × 6.8 × 8.5 nm with periodic boundary conditions. The temperature of 293 K was controlled employing the velocity rescale algorithm with the coupling constant of 0.5 ps (Bussi et al., 2007). The pressure was set to 1.013 bar and controlled in a semi-isotropic scheme using the Parrinello-Rahman barostat algorithm with a coupling constant of 10 ps (Bussi et al., 2007). The cut-off of 1.4 nm was used for both van der Waals and short-range Coulomb interactions whereas long-range electrostatics was accounted for by employing the Particle Mesh Ewald method (Essmann et al., 1995). All systems were simulated for at least 500 ns with the initial 300 ns treated as equilibration period and hence not used for further analysis. System equilibration was controlled by means of the standard convergence criteria for energy and temperature as well as by convergence of the area per lipid and by ensuring that bilayer properties (for instance, contacts of water and lipids with the peptide) are converged and similar in both bilayer leaflets. Equations of motion were integrated with 2 fs time step. All MD simulations were performed using the Gromacs 4.6.1 software suit and molecular visualization was done employing the VMD package (Hess et al., 2008, Humphrey et al., 1996).

All-atom molecular dynamics (MD) simulations: Analytical tools

Standard Gromacs tools together with in-house Python scripts were used for the analysis and visualization of the data with `NumPy` and `matplotlib` libraries being involved (van der Walt et al., 2011, Hunter, 2007). The ImageJ package was employed for the visualization of lateral densities (Schindelin et al., 2012).

Lateral diffusion maps were calculated independently for each bilayer leaflet by centering (during data post-processing) the amino acids that reside in proximity of the considered leaflet and then tracing the diffusion of lipids over an assumed time interval. The interval of 100 ns was chosen for the presentation purposes as it

corresponds to a relatively long-time diffusion and the obtained statistics is good for the 500 ns-long trajectories calculated here. Qualitatively the same results were obtained for 50 ns-long intervals.

For quantitative assessment of lipid mobility, we deliberately did not use mean square displacement and diffusion constants because we found a consistent estimation of these quantities in systems with and without peptide problematic. More specifically, MD simulations typically suffer from artificial drift of the center of mass of the studied system. This problem is even more pronounced for lipid bilayers as centers of mass of both leaflets usually drift laterally. A simple removal of such motion, independently for each leaflet, is a remedy even though not a perfect one. Of note, leaflets of lipid bilayers were experimentally shown to laterally slide with respect to each other and hence complete removal of their translational motion is not fully correct. In systems with a transbilayer peptide which couples both leaflets, it prohibits to some extent the lateral movement of leaflets with respect to each other but not the lateral movement of the bilayer as a whole. Overall, these differences between simulations of bilayers with and without transmembrane peptide make it very difficult to estimate and, in particular, quantitatively compare lateral diffusion under these two different conditions. Hence, we use autocorrelation function of lipid-lipid contact dynamics to access lipid mobility. This method provides values which are comparable between various simulated systems and does not suffer from the translational motion artifacts. Contact autocorrelation function C(t) is defined as:

$$C(t) = < A(\tau) - A(\tau + t) >_{\tau} \quad (10)$$

where the function A(t) gives the number of the considered interatomic contacts at time t and the averaging goes over time origins τ in the MD trajectory. The integral of the autocorrelation function over time is the contact correlation time. The decay of C(t) is related to the persistence of interatomic contacts, i.e., slowly-decaying contact autocorrelation function indicates longer-lasting atom-atom contacts. Here, C(t) was calculated employing the "-ac" option of the `g_hbond` Gromacs tool.

The average deuterium order parameters, S_{CD}, were calculated in both leaflets as arithmetic average of individual deuterium order parameters estimated for each carbon atom in sn-2 chains of DOPC using the standard `g_order` tool of Gromacs with the *"-d z"* option. Unsaturation of the two carbons in each chain was taken into account. For each carbon atom of a lipid acyl chain, the order parameter is calculated according to the equation:

$$S_{CD} = \langle 3 \cdot \cos^2 \theta_{C-D} - 1 \rangle / 2 \quad (11)$$

where $\theta_{C\text{-}D}$ is the angle between the bilayer normal and C-H bonds formed by the considered carbon atom. This parameter is standardly used for the characterization of membrane acyl chains in MD simulations, and it can be directly compared with the deuterium order parameter obtained from ^{2}H-NMR data (for more details see ref. (Vermeer et al., 2007)). The deuterium order parameter increases together with increasing acyl chain order.

Selection of annular and non-annular lipids was performed using the `g_select` tool of Gromacs. These two groups were defined employing the criterion of 0.75 nm lateral distance between any atom of a lipid and the peptide. The error of the average order parameter was estimated as the arithmetic average of errors (standard deviations) obtained for individual carbons using block averaging.

Radial distribution function (pair correlation function), g(r), gives a probability of finding the considered pair of molecules at the given distance r. Here, g(r) was calculated employing `g_rdf` Gromacs tool with the option "-rdf mol_com" to take into account distances between centers of masses of the considered molecules.

The error of the estimated time averaged values in MD simulations was calculated employing the block averaging method which accounts for fluctuations and autocorrelations while calculating the equilibrium

averages (Grossfield and Zuckerman, 2009). The Gromacs tool `g_analyze` with the "-ee" option was employed for this analysis.

Coarse grain molecular dynamics (CG-MD) simulations of the toy models of cylinder-like structures in lipid membranes

The toy models of cylinder-like structures in lipid membranes were prepared and simulated employing MARTINI force field (Marrink et al., 2007). A series of models with varying surface roughness were constructed. To this end, seventy MARTINI beads were packed into a space region corresponding to a cylinder with a diameter of 1.2 nm and a length of 4 nm using PACKMOL code (Martinez et al., 2009). This diameter equals to the diameter of helical peptide with an average backbone while the length was selected to allow the domain to span across DOPC lipid bilayer. The number of beads to be packed was chosen in order to obtain ~0.5 nm average distance between individual beads (approximately equal to the minimum inter-bead distance between the considered MARTINI beads). The packing resulted in a cylinder-like object comprising of closely packed MARTINI beads (model M1, see Figure 4A). Nine beads at both ends of the cylindrical domain were designed as polar, using P4 MARTINI bead type. The remaining 52 beads were designed as nonpolar, using C1 MARTINI bead type, the same as standardly used for nonpolar acyl chains of lipids. The resulting model of transmembrane domain had ~0.5 nm-long polar termini and 3 nm-long nonpolar central section; thus, resembling a typical short transmembrane helical peptide, such as LW21. Two toy models with increased surface roughness were generated by removal of randomly chosen 10 (model M2) and 26 (model M3) nonpolar beads (see Figure 4A). The elastic network method was employed with the elastic bond force constant set to 500 kJ mol^{-1} nm^{-2} and lower and upper elastic bond cut-off to 0.5 and 5.0 nm, respectively to preserve the structure of the toy models during MD simulations.

Simulations were performed with GROMACS 5.0.7 software package with standard parameters advised for MARTINI simulations (de Jong et al., 2016). Shortly, 1.1 nm cut-off was used for non-bonded interactions employing the potential-shift-Verlet method. The reaction-field algorithm was applied to account for long-range electrostatics with the relative electrostatic screening parameter of 15. Equations of motions were integrated with 10 fs time step. The temperature of 293 K was maintained using the velocity rescale algorithm with 1.0 ps coupling parameter and the pressure of 1 bar was controlled by the semi-isotropic Parrinello-Rahman thermostat with the coupling constant of 12. Trajectories of 1000 ns were calculated with first 200 ns of each simulation treated as equilibration. The toy models M1-M3 were embedded in a transmembrane orientation in previously equilibrated bilayers consisting of either 256 DOPC molecules (128 in each leaflet) or 256 DOPC with 80 molecules of cholesterol. The method of Javanainen was used for the embedding (Javanainen, 2014). The autocorrelation function of contacts between the beads of lipid tails and the surface of M1-M3 toy models were calculated in the same way as in the case of all-atom MD simulations for membranes without and with cholesterol (Figures 4B and S9).

Supplemental References

BENDA, A., BENES, M., MARECEK, V., LHOTSKY, A., HERMENS, W. T. & HOF, M. 2003. How to determine diffusion coefficients in planar phospholipid systems by confocal fluorescence correlation spectroscopy. *Langmuir,* 19**,** 4120-4126.

BUSSI, G., DONADIO, D. & PARRINELLO, M. 2007. Canonical sampling through velocity rescaling. *J Chem Phys,* 126, 014101.

DE JONG, D. H., BAOUKINA, S., INGOLFSSON, H. I. & MARRINK, S. J. 2016. Martini straight: Boosting performance using a shorter cutoff and GPUs. *Comput Phys Comm,* 199**,** 1-7.

ESSMANN, U., PERERA, L., BERKOWITZ, M. L., DARDEN, T., LEE, H. & PEDERSEN, L. G. 1995. A Smooth Particle Mesh Ewald Method. *J Chem Phys,* 103**,** 8577-8593.

FEE, R. S. & MARONCELLI, M. 1994. Estimating the Time-Zero Spectrum in Time-Resolved Emission Measurements of Solvation Dynamics. *Chem Phys,* 183**,** 235-247.

GROSSFIELD, A. & ZUCKERMAN, D. M. 2009. Quantifying Uncertainty and Sampling Quality in Biomolecular Simulations. *Ann Rep Comput Chem, Vol 5,* 5**,** 23-48.

HESS, B., KUTZNER, C., VAN DER SPOEL, D. & LINDAHL, E. 2008. GROMACS 4: Algorithms for highly efficient, load-balanced, and scalable molecular simulation. *J Chem Theory Comput,* 4**,** 435-447.

HORNG, M. L., GARDECKI, J. A., PAPAZYAN, A. & MARONCELLI, M. 1995. Subpicosecond Measurements of Polar Solvation Dynamics - Coumarin-153 Revisited. *J Phys Chem,* 99**,** 17311-17337.

HUMPHREY, W., DALKE, A. & SCHULTEN, K. 1996. VMD: Visual molecular dynamics. *J Mol Graphics & Model,* 14**,** 33-38.

HUNTER, J. D. 2007. Matplotlib: A 2D graphics environment. *Comput Sci & Engin,* 9**,** 90-95.

JAMBECK, J. P. & LYUBARTSEV, A. P. 2012. An Extension and Further Validation of an All-Atomistic Force Field for Biological Membranes. *J Chem Theory Comput,* 8**,** 2938-48.

JAVANAINEN, M. 2014. Universal Method for Embedding Proteins into Complex Lipid Bilayers for Molecular Dynamics Simulations. *J Chem Theory Comput,* 10**,** 2577-2582.

JAVANAINEN, M. & MARTINEZ-SEARA, H. 2016. Efficient preparation and analysis of membrane and membrane protein systems. *Biochim Biophys Acta,* 1858**,** 2468-82.

KAISER, H. J., ORLOWSKI, A., ROG, T., NYHOLM, T. K., CHAI, W., FEIZI, T., LINGWOOD, D., VATTULAINEN, I. & SIMONS, K. 2011. Lateral sorting in model membranes by cholesterol-mediated hydrophobic matching. *Proc Natl Acad Sci U S A,* 108**,** 16628-33.

KAWATO, S., KINOSITA, K. & IKEGAMI, A. 1977. Dynamic Structure of Lipid Bilayers Studied by Nanosecond Fluorescence Techniques. *Biochemistry,* 16**,** 2319-2324.

KINOSITA, K., IKEGAMI, A. & KAWATO, S. 1982. On the Wobbling-in-Cone Analysis of Fluorescence Anisotropy Decay. *Biophys J,* 37**,** 461-464.

MACHAN, R. & HOF, M. 2010. Lipid diffusion in planar membranes investigated by fluorescence correlation spectroscopy. *Biochim Biophys Acta,* 1798**,** 1377-91.

MARRINK, S. J., RISSELADA, H. J., YEFIMOV, S., TIELEMAN, D. P. & DE VRIES, A. H. 2007. The MARTINI force field: Coarse grained model for biomolecular simulations. *J Phys Chem B,* 111**,** 7812-7824.

MARTINEZ, L., ANDRADE, R., BIRGIN, E. G. & MARTINEZ, J. M. 2009. PACKMOL: A Package for Building Initial Configurations for Molecular Dynamics Simulations. *J Comput Chem,* 30**,** 2157-2164.

SCHINDELIN, J., ARGANDA-CARRERAS, I., FRISE, E., KAYNIG, V., LONGAIR, M., PIETZSCH, T., PREIBISCH, S., RUEDEN, C., SAALFELD, S., SCHMID, B., TINEVEZ, J. Y., WHITE, D. J., HARTENSTEIN, V., ELICEIRI, K., TOMANCAK, P. & CARDONA, A. 2012. Fiji: an open-source platform for biological-image analysis. *Nat Methods,* 9**,** 676-82.

SORIN, E. J. & PANDE, V. S. 2005. Exploring the helix-coil transition via all-atom equilibrium ensemble simulations. *Biophys J,* 88**,** 2472-2493.

STOCKL, M. T. & HERRMANN, A. 2010. Detection of lipid domains in model and cell membranes by fluorescence lifetime imaging microscopy. *Biochim Biophys Acta*, 1798, 1444-1456

VAN DER WALT, S., COLBERT, S. C. & VAROQUAUX, G. 2011. The NumPy Array: A Structure for Efficient Numerical Computation. *Comput Sci & Engin,* 13**,** 22-30.

VEGA, C. & DE MIGUEL, E. 2007. Surface tension of the most popular models of water by using the test-area simulation method. *J Chem Phys,* 126, 154707.

VERMEER, L. S., DE GROOT, B. L., REAT, V., MILON, A. & CZAPLICKI, J. 2007. Acyl chain order parameter profiles in phospholipid bilayers: computation from molecular dynamics simulations and comparison with H-2 NMR experiments. *Eur Biophysics J,* 36**,** 919-931.

VIT, O., MAN, P., KADEK, A., HAUSNER, J., SKLENAR, J., HARANT, K., NOVAK, P., SCIGELOVA, M., WOFFENDIN, G. & PETRAK, J. 2016. Large-scale identification of membrane proteins based on analysis of trypsin-protected transmembrane segments. *J Proteom,* 149**,** 15-22.